UNIVERSITÀ DEGLI STUDI DI PADOVA

DIPARTIMENTO DI INGEGNERIA INDUSTRIALE

Tesi di Laurea Magistrale in

Ingegneria Chimica e dei Processi Industriali

MicroGasic: Hydrodynamic study and design of a micro-reactor for gas-solid reactions in absence of catalyst support material

Relatore: *Prof. Andrea Claudio Santomaso*

Correlatore: *Prof. Nouria Fatah*

Unité de Catalyse et Chimie du Solide - École Centrale de Lille

Laureando: Marco Menegus

ANNO ACCADEMICO 2013-2014

Alla mia famiglia

Summary

The advantages of micro-fluidized beds have been studied in detail for A, B and D Geldart's group powders and for larger particles diameters and are well known in scientific literature. Nowadays, it is interesting to investigate smaller particle diameters to better understand the dynamics and the behaviour of finer powders. It is for this reason that this study is focused on C Geldart's group particles.

This project aims to realize a micro-fluidized bed charged with micro and nano-powders and to set up a diagnostic methodology to understand and characterize the flow regime inside the vessel. The work has been performed on three prototypes with different internal diameter; the results obtained with the first one have been the basis to design the second and the third one. Starting with 340 μm powders and an internal diameter for the column of 8 mm, for the first prototype; finally, it has been possible to reduce the size up to360 nm powders and a vessel with 1mm of internal diameter with the third prototype.

This project is the extension of the microfluidic concepts, generally applied to liquid phases, which have been implemented to powder fluidization.

Moreover, a diagnostic methodology based on the analysis of the time fluctuations in the pressure drop has been realized. Thanks to this, the detection of the flow regime permits to avoid some drawbacks of the fluidization (such as channeling, slugging and caking) in order to achieve the best contact between the phases and the best mass and heat transfer.

INDEX

Introduction

The design of novel micro-reactors (microgasic systems) has demonstrated its potential and its interest in numerous branches of industry. Currently, a lot of reactors is very large in size and uses particles with low surface area which requires high gas velocity. This leads to large quantity of waste resulting into high cost of waste and energy. In the current socio-economic context, it is necessary to reduce the size of the reactor to decrease the quantity of waste and the energy for the production of solids. Novel microreactors with unique design can be efficiently used for a large number of applications in environmentally friendly processes.

This project aims to design a new reactor in respect of the environment which could have many applications such as the conversion of syn-gas to ultra clean hydrocarbon fuels and, in general, the improvement of catalytic reactions.

The project has been carried out as follows:

- Study of micrometric and nanometric powders behaviour on the first prototype for the microgasic reactor
- Calculation of minimum fluidization speed from mathematical equation
- Development of the second prototype for the microgasic reactor
- Study of the Hydrodynamic behaviour (gas-solid)
- Design and development of the third prototype for the microgasic reactor
- Implementation of a diagnostic methodology to determine the flow regime
- Study of the feasibility and the validity of the concept

The present work is structured as follows: there is a first chapter on fluidization basic concepts and related phenomena which take place in fluidized beds. Then, a chapter on the design and realization of the prototypes explains the steps which have been followed to create a micro-fluidized bed. A third chapter is dedicated to the hydrodynamics study which has been performed on different powders in the second prototype. Finally, conclusions and future possible improvements are described in chapter 4 and 5.

1 CHAPTER ONE
PHENOMENA IN FLUIDIZED BED REACTORS

The solid fluidization consists of a process in which a gas phase and a solid granular phase (the particles) are put in deep contact. The solid phase is held up by a support which has also the function of a gas distributor (see Fig. 1.1). By sending a gas flow directed upwards from the lower base of the vessel, this exerts a drag force on the particles which increases with the gas speed. And as this speed increases, different phenomena can take place and different flow regimes can be identified.

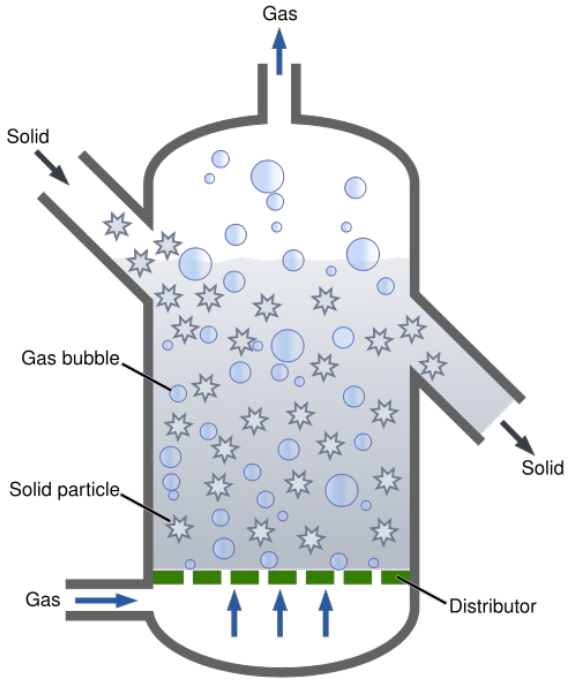

Fig. 1.1 Schematic of a fluidization process.

The powder is charged from the upper inlet on the left side of the vessel, while the gas is sent in from the bottom of the unit through a specific inlet tube.
In this case the powder can go out from the vessel from the outlet on the right side of the unit, but in other applications the same powder is kept inside the vessel and reused several times.

1.1 Geldart's classification criterion

During the laboratory experiments performed in this project, several powders have been used; these have been classified according to Geldart's criterion [1].
This classification is based on the influence which each powder has on the hydrodynamics of fluidized bed and it distinguishes four groups (A, B, C and D) examining the density and the average diameter of each powder.

A powders are aeratable, having small particles and low density they allow high expansion of the bed.

On the other hand, ***B*** ones are similar to sand and allow lower bed expansion but in presence of bubbles.

C ones are very cohesive and are likely to agglomerate, in this way it is very common to see preferential channels in the bed. The gas passes through this channels and so the bed expansion is limited.

Finally, ***D*** powders are larger in diameter and tend to create a turbulent flow regime in the bed.

Geldart's classification also considers the gas fluidization properties and its density (see Fig. 1.2).

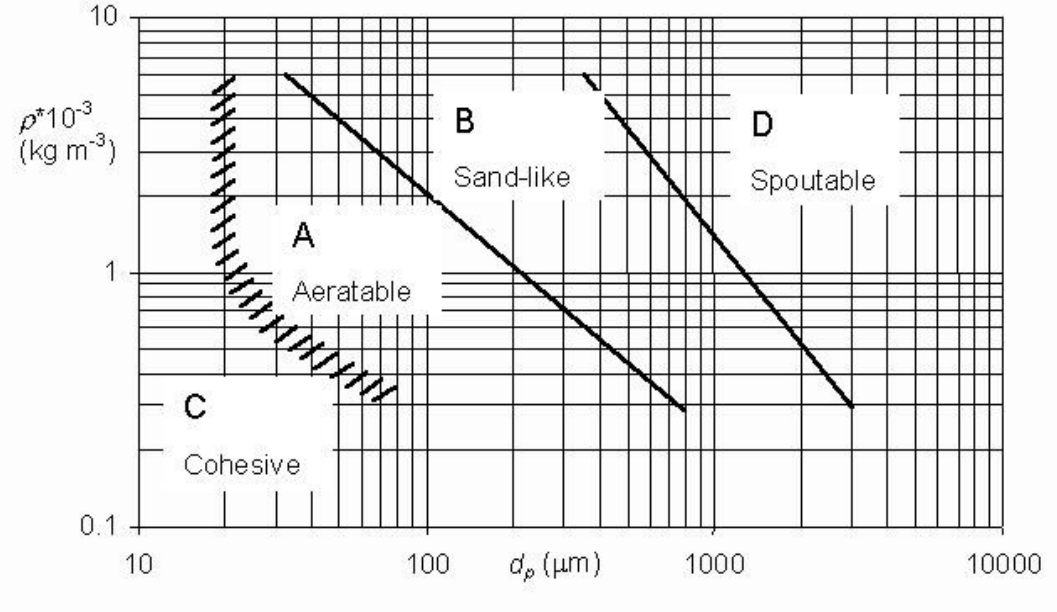

Fig. 1.2 Chart for characterizing different powders by D. Geldart.

1.2 The fixed bed regime

For small values of the gas speed, the solid particles are not affected by the gas flow and they stand still, letting the gas pass through the empty spaces between the particles; this is called the fixed bed regime.

In this case the bed expansion is absent and the porosity has constant value; the measured pressure drop increase with the gas flow rate.

In order to better understand the dynamics inside the fluidization unit, it is be useful to measure and plot the pressure drop inside the particle bed varying the gas speed.

In particular, for a normal fluidized bed we expect to have a plot similar to the one in Fig. 1.3. In fact, we can observe a first part of the curve having a certain slope and a second part with constant ΔP value.

The first part of the curve represents the fixed bed regime; for a known value $U < U_{mf}$, ΔP increases with U, but the particles are not moved by the gas flow. The second one represents the fluidized bed regime; for $U > U_{mf}$, ΔP is constant as the gas flows

through the solid phase moving the particles in the expanded bed.

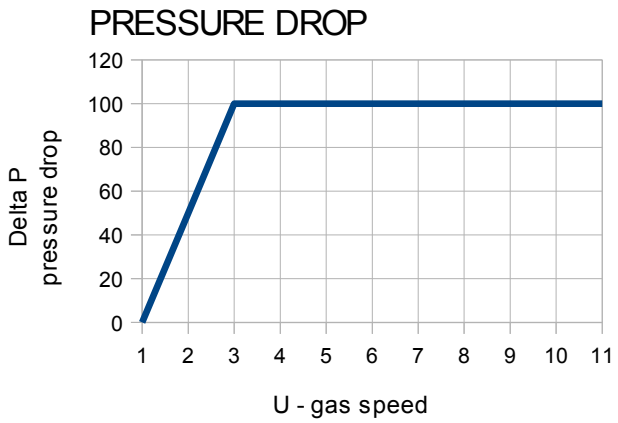

Fig. 1.3 Typical plot of pressure drop vs gas speed for a normal fluidized bed

As the gas speed increases, the drag forces reach higher values and the particles begin to move in order to attain the minimum resistance which they can oppose to the gas flow.
When the drag forces are high enough to balance the weight of the particles, the whole bed behaves like a fluid (see Fig. 1.4).
The minimum fluidization speed U_{mf} is then reached and the fluidized bed regime occurs. At this point small empty zones can be seen just over the gas distributor and, since they are composed of pure gas, they are called *bubbles*.
If we increase the gas speed to even higher values, we can obtain different flow regimes in the bed.
It is recommended to use this operational values for the gas flow rate and thus for U_{mf}:

- $U = 1{,}5 \div 5 \cdot U_{mf}$ *for A, B, D Geldart's group powders*
- $U = 2 \div 100 \cdot U_{mf}$ *for C Geldart's group powders* .

If we use multiples of U_{mf}, we could have higher values in the bed height and a more

expanded particle active layer.

As the gas speed keeps increasing, each particle begins to move according to its weight; the smaller ones (and so the lighter) reaches more easily the top of the active layer, while the bigger ones (having higher weight) will tend to rapidly fall again on the grid supporting the solid material.

In this way the active layer is continuously renewed and the position of the particle will continue to change from the upper to the lower part of the fluidized bed.

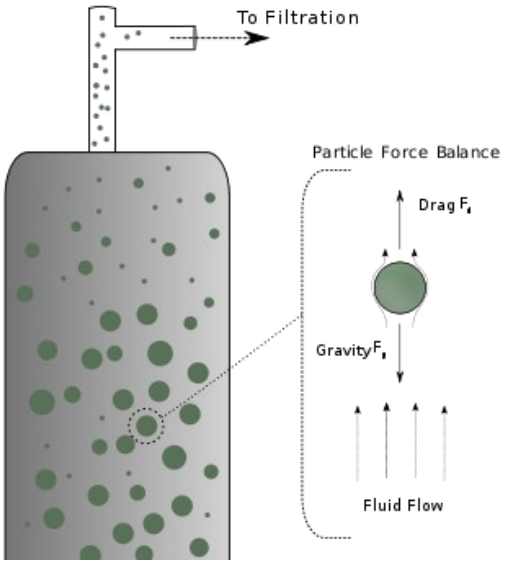

Fig. 1.4 Particular of the upper part of a fluidization vessel with the force balance for a single particle .

[2]

In Fig. 1.5 it is shown another plot (analogue to the one for fluidized bed) for a normal entrained bed; in this case we can see that the pressure drop after rising and being constant, it can decrease. This phenomenon occurs after all the particles have been carried out of the unit from the gas flow.

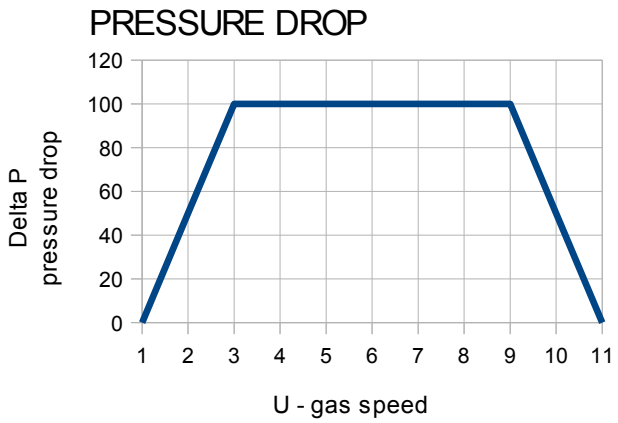

Fig. 1.5 Typical plot of pressure drop vs gas speed for an normal entrained bed

As a lower number of particles is present in the bed, the resistance opposed to the gas flow will be lower. Thus the value of the pressure will decrease until all the particles have been transported out of the vessel.

1.3 The boiling bed regime

When the gas is present in form of bubbles, the flow regime is thus called *the boiling bed regime,* due to its similarity to a boiling liquid.

This situation can be observed for $U > U_{mf}$ when small bubbles form just over the gas distributor and raising through the bed height they grow in dimension thanks to coalescence phenomena. In this regime, the porosity and expansion of the bed are not constant anymore and they increase with the gas speed. The upper surface of the bed is rippled by the bubbles raising from the bottom of the bed itself.

1.4 The slugging regime

While working with very cohesive powders, it can be noticed that the particles tend to move in clusters, in other words, they will aggregate in irregular shapes behaving like bigger particles. If the cohesive strengths are very high, the clusters can reach important dimensions and tend to move as layers which can have big height compared to the total bed height. This layers will move alternatively up and down, suspended by the air flowing inside the bed. This flow regime is called *the slugging regime,* in fact, the layers can have the shape of a disk as large as the cross-sectional area of the reactor and they are similar to a piston. This regime will be discussed again in section1.7.2.

1.5 The turbulent regime

If the gas speed is further increased, likewise in liquid systems, the turbulent regime can be reached. This regime can be detected when the bubble size decrease with the gas flow rate and an intensive mixing in the solid phase. In the following picture different flow regimes of fluidization are shown.

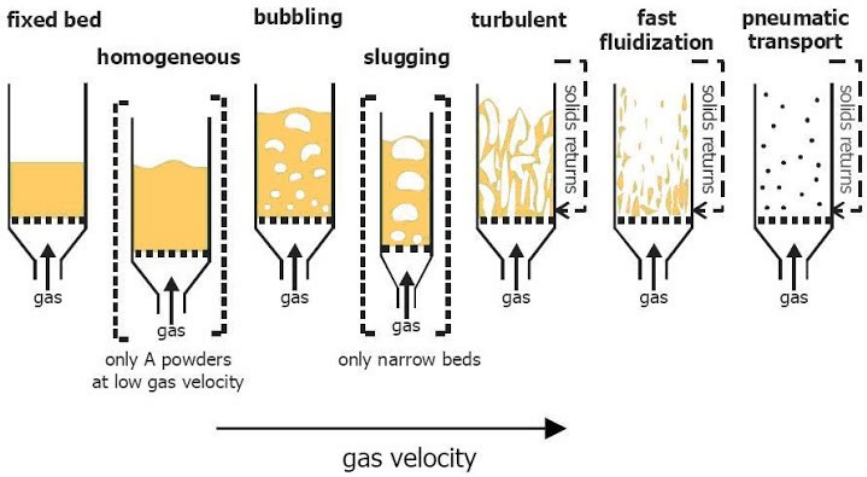

Fig. 1.6 The different fluidization regimes .

[3]

1.6 Flow regimes characterization

As already said, after the minimum fluidization point (in correspondence of U_{mf}), two slightly different kinds of fluid flow can be observed: the *particulate* and the *aggregative* fluidization.

In the first case the bed behaves in a uniform manner: and increasing the flow rate the bed height increases; hence, the increasing fluid flow simply goes to expand the bed.

In the second case, also named *bubbling,* aggregates of fluid may be observed within the fluidized bed that move rapidly to the surface.

To determine if a bed will bubble or not there is a simple criterion based on the Froude number.

$$Fr = \frac{U_{mf}^2}{d_p \cdot g} \tag{1}$$

where d_p is the particle diameter and g is the gravity acceleration.

For $Fr > 1$ bubbling is more likely to appear. To have a more precise criterion also the Reynolds number for the particles, the density ratio and the bed ratio can be introduced. The Reynolds number for the particles is defined as follows:

$$Re_p = \frac{d_p U_g \rho_g}{\mu_g} \tag{2}$$

where d_p is the particle diameter, U_g is the gas speed, ρ_g is the air density and μ_g is the air viscosity.

The density ratio and the bed ratio are defined as follows:

$$density\ ratio = \frac{\rho_s - \rho}{\rho};\quad bed\ ratio = \frac{H_{mf}}{d_r} \tag{3}$$

where H_{mf} is the bed height at minimum fluidization and d_r is the bed diameter.

Thus, the correlations for this criterion are :

$$Fr \cdot Re_p \cdot \left(\frac{\rho_s - \rho}{\rho}\right) \cdot \left(\frac{H_{mf}}{d_r}\right) < 100 \qquad particulate\ fluidization \qquad (4)$$

$$Fr \cdot Re_p \cdot \left(\frac{\rho_s - \rho}{\rho}\right) \cdot \left(\frac{H_{mf}}{d_r}\right) > 100 \qquad bubbling\ fluidization \qquad (5).$$

According to Geldart's [1] classification, it can be said that Group A powders may not bubble, if it does then bed will expand before bubbling; in general, they may have fast moving bubbles with dimension lower than 100 mm.
Groups B and D powders will show large bubbles and they may form slugs. Group D powders normally give slow bubbles, while group C ones, being very cohesive, they will have high inter-particle forces which will lead to difficult
fluidization, an they will more likely form channels or slugs instead. [4] [5]

According to Clift [6] and Rafailidis [7] when bubbling fluidization does occur, experimental works have shown that inter-particle stresses actually play a fundamental role in bubble wakes while, for group A, B and D solids, inter-particle stresses play a secondary role elsewhere and can in general be neglected to a first approximation.
Loosely speaking, the motion of bubbles, once they have been formed, is insensitive to the rheological properties of the dense phase. Clift (1993) showed, on the other hand, that to explain the pre-bubbling differences between group A and B powders, one must consider inter-particle forces, in particular the elasticity of the particulate phase which is critically dependent on particle-particle contacts.

1.7 Inconveniences in fluidized beds

When performing fluidization in a vessel some inconvenience can occur. In particular these are *channeling, slugging* and some phenomena related to friction.

1.7.1 The channeling phenomenon in fluidized beds

This inconvenience can occur especially working with very cohesive powders, in fact, it is very common to experience it with the powders of C Geldart's group. In general channeling is more likely to occur when the diameter of the particles is d_P<50 μm.

The buoyancy forces deriving from the gas flowing from the bottom of the vessel are not sufficiently strong to overcome the cohesive forces between the particles. Thus, for values of the gas flow which permit a good level of fluidization when working with powders of other groups, a fixed bed regime is experienced. Increasing the gas speed to higher values causes the formation of preferential channels in the bed (Fig. 1.7). This channels became the only way for the gas to pass through the bed as they offer minimum resistance against the gas flow.

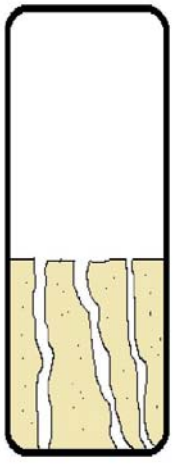

Fig. 1.7 Schematic representation of the channeling phenomenon in fluidized beds.

When channeling occurs, the worst level of mixing and the lowest fluidization quality are

achieved as there are zones which are completely not interested by the passage of the gas phase. It is therefore a situation to strongly avoid in a fluidized bed, especially if the purpose is to perform chemical reactions.

1.7.2 The slugging phenomenon in fluidized beds

The slugging phenomenon is often experienced when working with very cohesive powders and especially with narrow columns, in particular, columns which have an aspect ratio $Hfc/D_r > 1$.

When these conditions are verified, the particles tend to create clusters. If the cohesive strengths are very high, the clusters can be large in dimension and tend to be floated by the gas bubbles coalescing under them. This layers will move alternatively up and down similarly to a piston, and since they form, it is very difficult that they can be deagglomerated by the flow (Fig. 1.8).

As stated for the channeling, even with the slugging a very bad level of mixing and low fluidization quality are achieved.

In fact, in this case there are zones of the bed which are completely segregated and tend to be in the same conditions even with strong gas flow-rates. The slugging is a phenomenon which has to be avoided in a fluidization process, as mass and heat transfer and, in general, the quality of a chemical reaction can be really compromised.

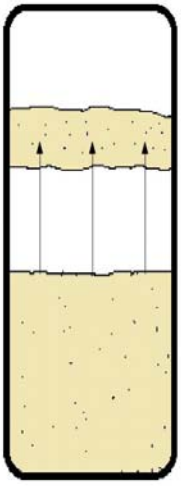

Fig. 1.8 Schematic representation of the slugging phenomenon in fluidized beds.

1.7.3 Three phenomena related to friction in fluidized beds

In fluidized beds friction forces can reach high values. There are three main inconveniences which are related to friction that can occur in a fluidization vessel: *abrasion*, *fragmentation* and *chipping* (see Fig. 1.9).

When smaller particles hit a bigger one in the flow, the friction forces are so high that they can damage the surface of the bigger particle. If the particle is the catalyst this can cause a decrease in the global performance of the chemical reaction.

Similarly, collision between to big particles can lead to rupture of the particle itself and to the formation of smaller fragments. In this case, a variation in the diameter distribution can be experienced, as the number of particles with lower diameter increase.

Finally, chipping can occur when a particle loses a flat section from its surface due to some collision or other frictional stresses.

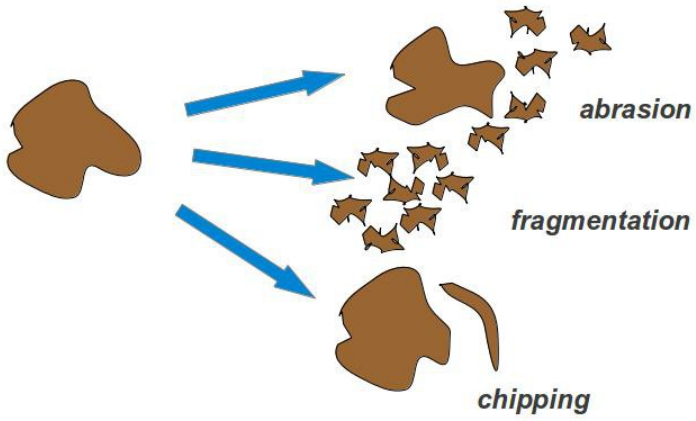

Fig. 1.9 Phenomena related to the friction between particles : abrasion, fragmentation and chipping.

1.8 Bibliography research: previous works on similar subjects

Here, in Tab. 1.1 it is shown a review of previous works on fluidization found in the scientific literature; this has been a first step to understand the main phenomena and prepare the experimental work.

Tab. 1.1: Summary table for the bibliography research (see5.1for detailed notes).

Authors	***Materials***	***Diameters***	***Parameters***	***Purposes***
B. Potic, S.R.A. Kersten, M. Ye, M.A. van der Hoef, J.A.M. Kuipers, W.P.M. van Swaaij. [8]	Sand 2450 kg/m^3	$60-70\,\mu m$ $80-90\,\mu m$ $100-150\,\mu m$ $150-250\,\mu m$	D_r=1mm U_{mf} U_t	Applications for biomass gasification
Xinhua Liu, Guangwen Xu , Shiqiu Gao. [9]	Sand, Silica	$96\,\mu m$ $242\,\mu m$ $460\,\mu m$	U_{mf}, U_{mb}	Find the optimal combination between: D_r and D_p
Ma Jiliang, Chen Xiaoping, Liu Daoyin. [10]	Quartz sand, bottom ash 2750 kg/m^3 and 2500 kg/m^3	1,29mm (quartz) 0,5mm (bottom ash)	T_b, U_{mf}	Explore the effects of bed temperature and PSD on U_{mf}
Rossella Girimonte, Vincenzino Vivacqua [11]	glass ballotini, ceramic, zirconium oxide, steel and bronze spheres	$0.41\,cm$ $1.1\,cm$ $100-588\,\mu m$	H_{fc}/D_r , U_{mf}, ε	Find fixing criteria to obtain a regime of homogeneous fluidization

1.9 Physical definitions

A first set of measures was performed after some theoretical calculations have been done.

To better characterize the dynamics of the fluidized bed it is useful to consider the Reynolds number for particles (2). In particular, Reynolds number can be calculated in minimum fluidization conditions (Re_{mf}) to quantify the state of a fluidized bed in which the air sent in has the power to move only the upper part of the powder layer.

Re_{mf} is calculated with U_{mf}, gas speed in minimum fluidization and it is defined as follows:

$$Re_{mf} = \frac{d_p U_{mf} \rho_g}{\mu_g} \quad . \qquad (6)$$

On the basis of Wen & Yu relation [12](7), the Reynolds number in minimum fluidization conditions can be obtained.

$$Re_{mf} = (33{,}7^2 + 0{,}0408 \cdot Ar)^{1/2} - 33{,}7 \quad . \qquad (7)$$

Where Ar is the dimensionless number of Archimedes and it is defined as follows:

$$Ar = \frac{\rho_g \cdot d_p^3 \cdot (\rho_p - \rho_g) g}{\mu_g^2} \quad . \qquad (8)$$

From the previously calculated value of Re_{mf}, in this way U_{mf} can be easily obtained reversing the equation number (6). The minimum fluidization speed has been taken as a reference value for the set of measurements performed for each powder studied.

Another value for the speed has been taken into account as an upper limit for the fluidization. The maximum limit speed U_t has been calculated through the following formulas:

$$U_t = \frac{(\rho_p - \rho_g) \cdot g\, d_p^2}{18 \mu_g} \qquad Re < 2 \qquad (9)$$

$$U_t = \left(\frac{1{,}78 \cdot 10^{-2} (\rho_p - \rho_g)^2 \cdot g^2 d_p^3}{\rho_g \mu_g} \right)^{1/3} \qquad 2 < Re < 500 \quad . \quad (10)$$

The operating speed for the gas has been chosen in this way:

$$U_{mf} < U < U_t \quad . \qquad (11)$$

Another important parameter has to be defined to describe the quality of the fluidization. In ideal conditions, in which the bed is completely fluidized, the pressure drop is equal to the apparent weight of the particles divided for the cross sectional area:

$$\Delta P_{mf} = \frac{W}{A} \quad . \qquad (12)$$

Thus, we can use the ratio between the pressure drop and the apparent weight per unit of surface as a parameter describing how far we are from the theoretical unit value, as shown in formula (13):

$$fluidization\ quality\,(\%) = \frac{\Delta P}{W / A} \qquad (13).$$

1.10 Considerations on the shape of the particles

1.10.1 Sphericity

An important issue to be considered is the shape of the particles we are working with. In fact, the shape has a great influence in the dynamics of the the solid phase. Sphericity is a measure of how spherical an object is; in other words, if the object is not a perfect sphere, it measures how far the shape of that object is from the spherical one. The spherical factor Ψ is defined in the following formula:

$$\Psi = \frac{\pi^{\frac{1}{3}}(6\ V_p)^{\frac{2}{3}}}{A_p} \qquad (14)$$

where V_p is the volume of the particle and A_p is the area of the surface of that particle.

This imply that $\Psi = 1$ only for perfect spheres, while $\Psi < 1$ for all non-spherical objects. During the experiments, for all the glass particles, since they nominally have spherical shape, $\Psi = 1$ has been assumed.

1.10.2 Equivalent diameter

Considering different properties of a particle (say surface area, volume, projected area etc.) several equivalent diameters can be defined and calculated. The real particle can be compared to an ideal geometrical shape and a specific equivalent diameter can be defined with respect to a specific property of the real particle. For instance, we can compare the particles of a powder to spherical particles and then calculate the respective equivalent diameter taking into account the specific area per volume that the particle has. The equivalent diameter can be calculated from a comparison between the values of the specific area of the particle and the specific area of a sphere. As previously said, for the glass spheres this has not been necessary, while for the Titanium oxide (TiO_2) particles and Talc particles the diameter was known from experimental analysis.

2 CHAPTER TWO
MATERIALS AND METHODOLOGIES

2.1 The powders used in the experimental tests

For the first set of experiments six kind of powders have been chosen: glass spheres (with average diameter D_p=12 µm, D_p=63µm, D_p=157µm and D_p=340µm), Talc (with diameter D_p=12 µm) and Titanium oxide TiO_2 (with diameter D_p=360 nm). They represent the three groups A, B et C (see Fig. 2.1 and Tab. 2.1).

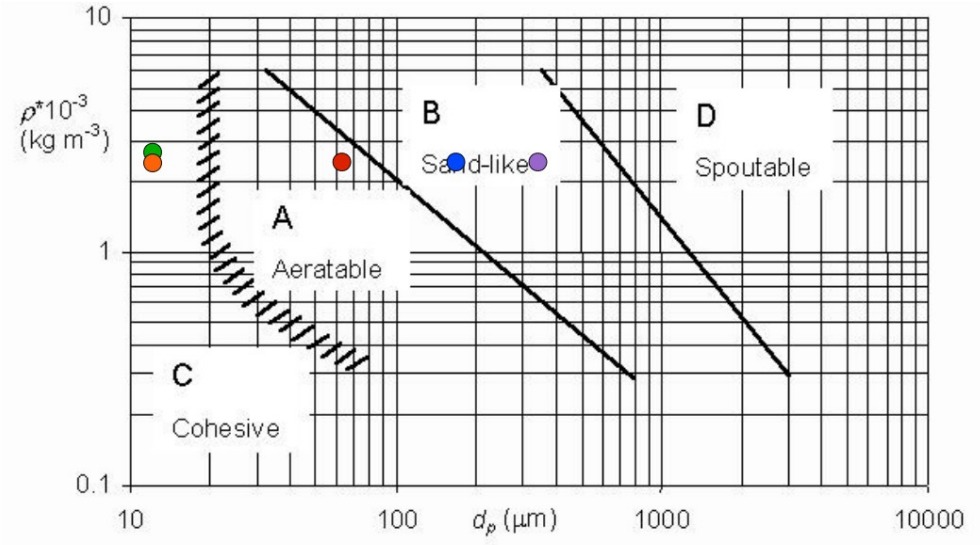

Fig. 2.1 Chart for characterizing different powders by D. Geldart (legend: green=talc, 12µm, 2700 kg/m³; legend: orange=glass, 12µm, 2640 kg/m³; red=glass, 63µm, 2640 kg/m³; blue=glass, 157µm, 2640 kg/m³; violet=glass,340µm, 2640 kg/m³).

Tab. 2.1 The different powders and their properties

	Group	***Diameter***	***Density [kg/m^3]***
Glass spheres 1	A	63 μm	2640
Glass spheres 2	B	157 μm	2640
Glass spheres 3	B	340 μm	2640
Glass spheres 4	C	12 μm	2640
TiO_2	C	360 nm	4200
Talc	C	12 μm	2700

2.2 Development of the MicroGasic reactor

In Fig. 2.2 it is shown a complete schematics of the fluidization unit with all the related devices. At the bottom it is shown the system for the compressed air with regulation valve, manometer to regulate the flow-rate, safety manometer to check the pressure values.

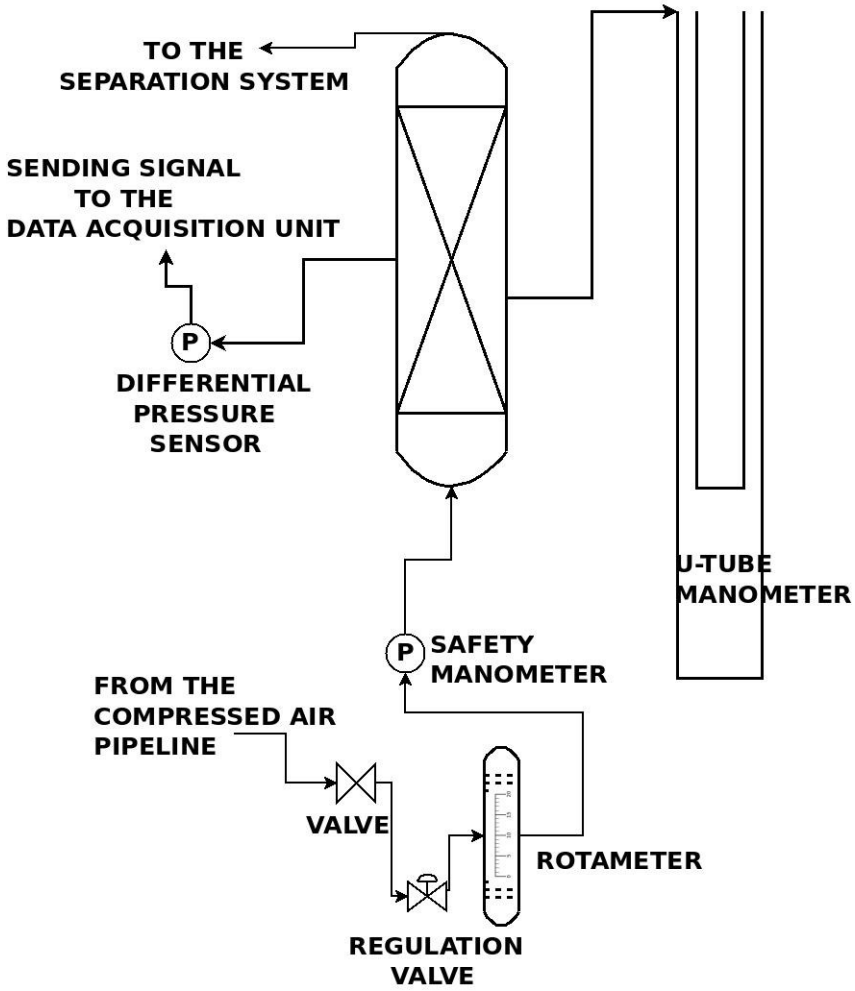

Fig. 2.2 Complete schematic of the fluidization unit with all related devices.

A U-tube manometer is connected to the unit to verify practically the values of the pressure drop inside the vessel; while an electronic differential pressure sensor is connected to the fluidized bed and then to an acquisition data system, to process and to examine the signal from the laboratory equipment.

This theoretical schematics has been the basis for the design and implementation of the three prototypes which are described in the following sections.

In the following paragraph are described the materials used for the experimental work.

2.3 The first prototype

The system used for the experiments is composed of a tube (length 55 cm with a 90° bend length 4,5 cm and interior diameter 8,5 mm) with 16 lateral tubes which can be used as pressure sockets (see Fig. 2.4).

This tube has two inlets at the bottom and one outlet in the upper part which is connected to a gas-powder separation system.

The two tubes at the bottom have the function of gas (i.e. compressed air) and powder inlet devices.

In the lower part of the unit, the powder is held up by a metallic grid which is put under the inlet tube for the powder phase. The grid has the function of supporting the fluidized bed.

A the top, the separation system is composed of a first vessel in which the gas-solid mixture speed is lowered. This vessel has the function of re-agglomerate the powders small in diameter so that a further separation from the gas phase is easily achievable. In fact, after that, a cyclone is found which separates the air from the solids at the top and another vessel which collects the powder accumulated in the cyclone (see Fig. 2.3 and Fig. 2.5).

Fig. 2.3 The separation system

Fig. 2.4 Apparatus for the experiments and manometers

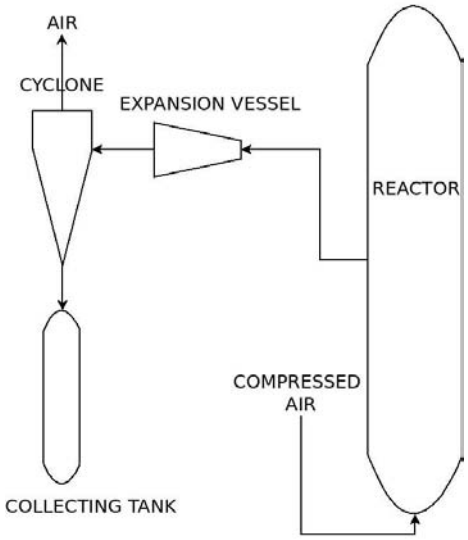

Fig. 2.5 Flow sheet related to the separation unit.

After some tests, it was necessary to close the supplementary pressure outlets and the lower tube used to send in the powder.

In fact, it was clear that there were powder losses in the lateral tubes and a dead volume in the main tube.

For this reason, a consistent part of the powder was accumulated at the mouthpiece of the main lateral tube and it did not take part to the fluidization process. Furthermore even in the pressure sockets there were little amounts of powder accumulating at the mouthpiece; in the final balance those mass losses had low influence indeed, but in order to protect the measuring system from the powder flowing inside the instrument tubes a different solution was needed.

Moreover, it was necessary to modify the grid in order to work with finer powders having smaller diameters.

The exam of these issues has been the starting point to the design of the second prototype.

2.4 The second prototype

The second prototype had the same dimensions of the previous one (lengths and internal diameter), but it was not equipped with pressure sockets neither with an inlet tube for powder (see Fig. 2.6 and Fig. 2.9). In particular in Fig. 2.6, the glass walls are marked in black, while the metal components of the pressure sockets are marked in red, the porous glass filter is marked in green and the measures (expressed in centimeters) are marked in blue; in Fig. 2.7 and Fig. 2.14 the schematic of the fluidized bed is shown in detail.

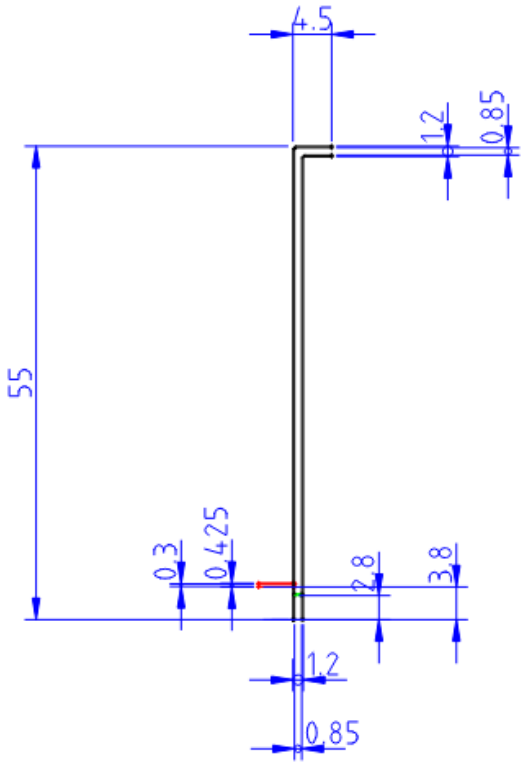

Fig. 2.6 Schematic of the second prototype (ref. measure cm).

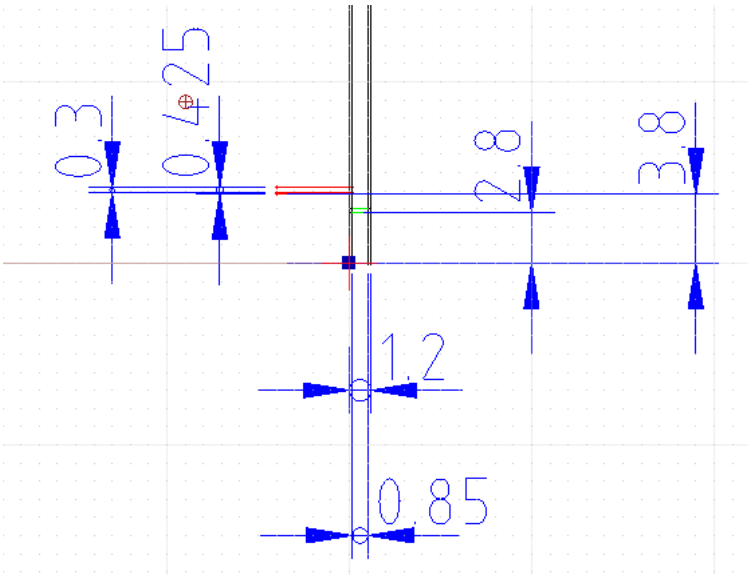

Fig. 2.7 Particular of the design schematic in the bottom of the second prototype: measures of the internal and external diameter and related to the pressure socket and porous glass (ref. measure cm).

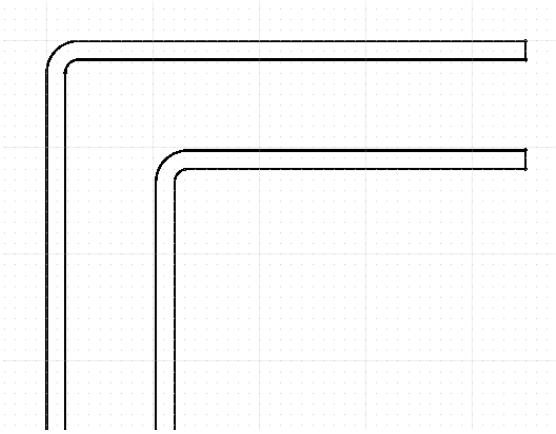

Fig. 2.8 Particular of the design schematic at the top of the second prototype: after a 90° bend the apparatus is connected to the separation unit.

In this case, the powder must be charged through the upper entrance and it is held up by a porous glass filter which is directly weld into the glass walls (see Fig. 2.10).

Fig. 2.10 Pressure socket and filter.

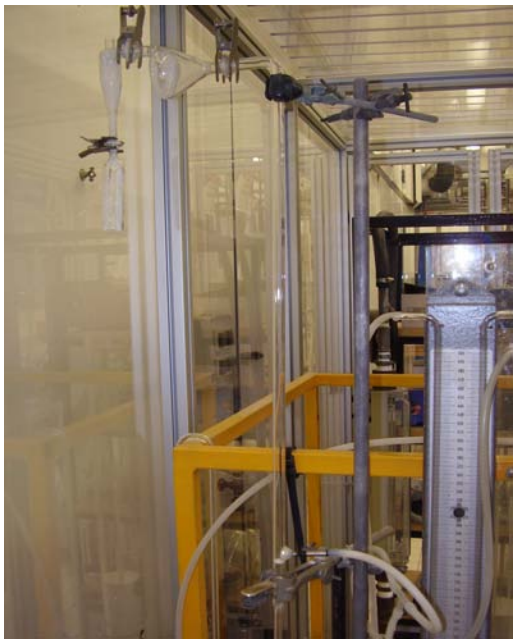

Fig. 2.9 The second prototype.

In order to measure the pressure drop the glass wall has been drilled and a pressure socket being flush with the wall has been installed just above the porous glass filter. The pressure socket is composed of two concentric steel tubes weld to a piece of metallic grid and made airtight with a heat-shrinkable material sleeve. The system is finally weld to the wall by a layer made of epoxy glue which makes the whole zone stable and airtight. Below this part, there is another tube to send in compressed air (see Fig. 2.11).

Fig. 2.11 Particular of the lower part of the apparatus: the compressed air inlet, the pressure socket and the porous glass filter.

2.5 The third prototype

Since the project aims to create a device that can be used in microfluidic applications, in the third prototype design, the internal diameter reached 1mm (see Fig. 2.12). Due to technical issues, the glass thickness had to be big in comparison to the internal channel; in this way the mechanical resistance of the structure wasn't compromised (Fig. 2.14 and Fig. 2.15).

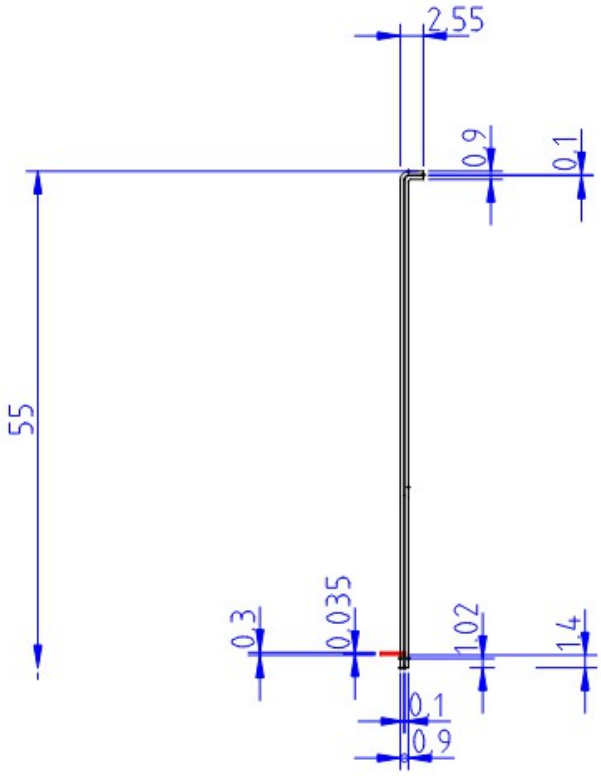

Fig. 2.12 Schematic of the third prototype (ref. measure cm).

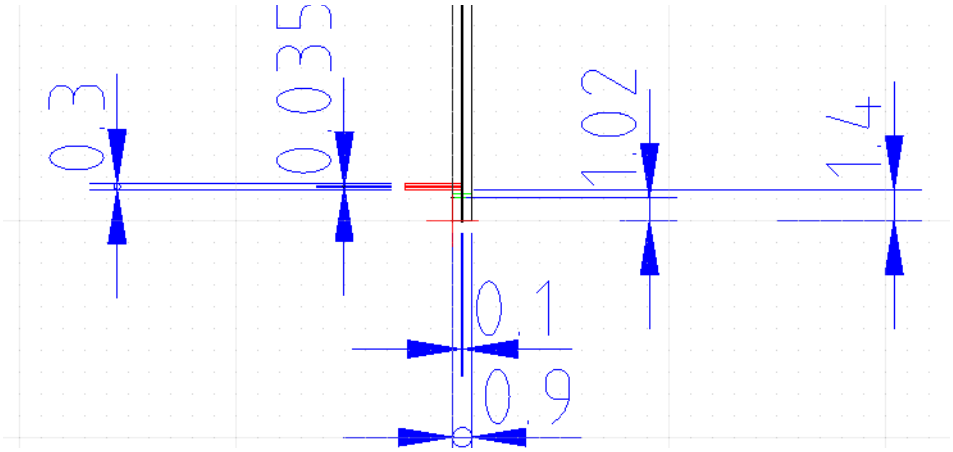

Fig. 2.13 Particular of the design schematic in the bottom of the third prototype: measures of the internal and external diameter and related to the pressure socket and porous glass (ref. measure cm).

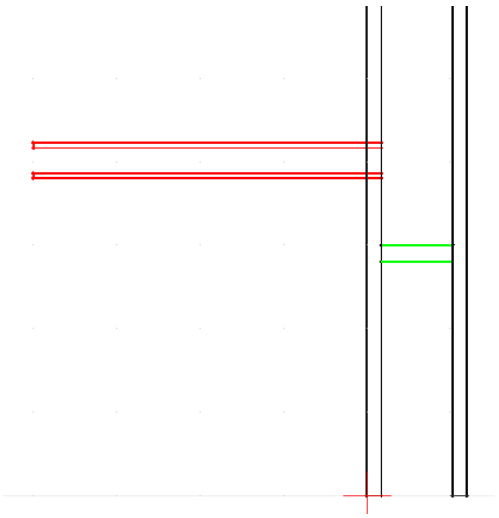

Fig. 2.14 Particular of the design schematic in the bottom of the second prototype: pressure socket (red) and porous glass filter (green).

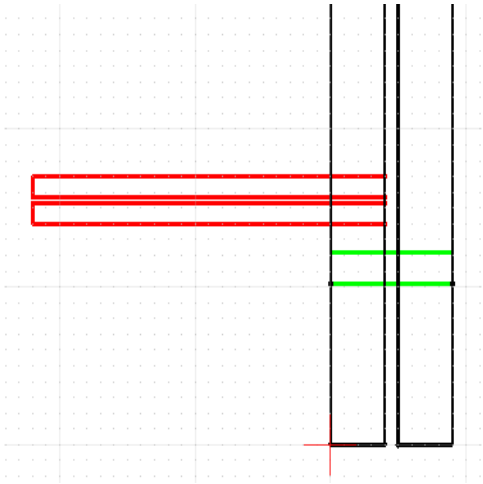

Fig. 2.15 Particular of the design schematic in the bottom of the third prototype: pressure socket (red) and porous glass filter (green).

In Fig. 2.14 and Fig. 2.15 it is clearly shown, the differences between the second and the third prototype. In the second prototype the internal diameter is 8,5mm, while in the third one it is 1mm.

Fig. 2.16 Particular of the connection piece: the internal metallic grid (40-100 μm)

Fig. 2.17:The connection piece from upper view: vertical internal channel and the lateral one for pressure drop measurement.

In order to insert a metallic tube for the pressure drop measurement within the fluidization bed, a connection piece has been designed. This piece in PVC material has been realized with a vertical internal channel of 1mm in diameter which is connected to the internal channel in the glass tube on the side of the plastic piece an horizontal lateral channel of 1 mm diameter and 2 mm in the final part, permits the insertion of a metallic tube (see Fig. 2.17). Inside the matrix of the plastic piece a metallic grid is installed to prevent fine powders to damage the instrumentation (see Fig. 2.16)

In Fig. 2.18 the whole third prototype is showed with the separation system connected at the top of the fluidization tube and the pressure socket connected to the measurement instrumentation.

The design of the internal channel has been performed considering that the external diameter of the glass structure needed to comply with the junction in the separation unit (see Fig. 2.19 and 2.20).

Fig. 2.18 Photograph of the third prototype;on the left side of the picture the separation system connected at the fluidization tube; on the right side of the picture the pressure socket connected to the measurement instrumentation.

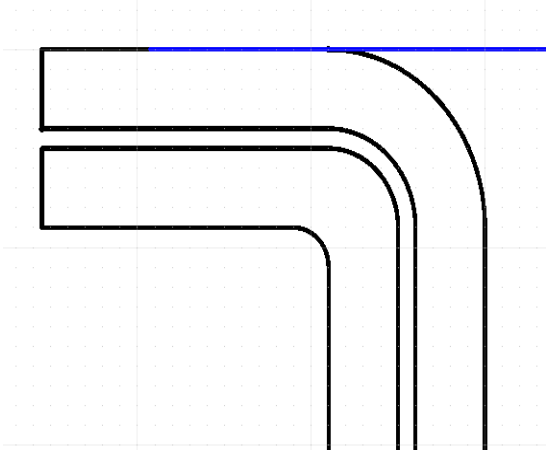

Fig. 2.19 Particular of the design schematic at the top of the third prototype: after a 90° bend the apparatus is connected to the separation unit.

Fig. 2.20 Photograph of the top of the third prototype, the tube had to be enlarged in the ending part to permit the connection to the following separation system.

In Fig. 2.21 it is shown a particular of the bottom of the fluidization unit with the PVC connection piece installed inside the glass matrix. It can be seen in detail, from a side view, the filter and the metallic pressure socket.

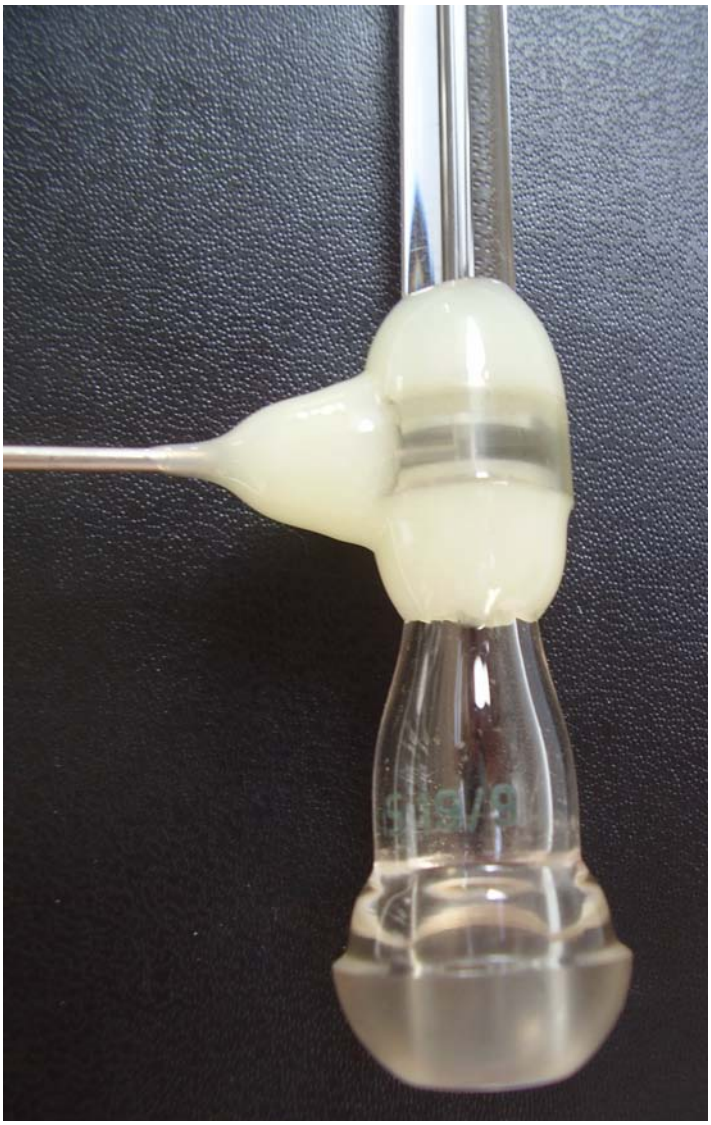

Fig. 2.21 Photograph of the bottom of the third prototype: installation of the connection piece with filter and pressure socket .

2.6 Data measurement and acquisition unit

Since the project aims to carry out the diagnostic of the dynamics regime in the reactor based on pressure measures, it has been necessary to set up an adequate measuring system. In Fig. 2.22 it is showed the differential pressure sensor, its power supply unit and a connected voltmeter unit.

The pressure measured is transferred in the form of electrical signal and it has to be known that 1mbar (i.e. 10mm water column in the manometer) corresponds to 0,1V. In Fig. 2.23 it is shown the data acquisition unit which was connected to a computer and which permitted a direct monitoring of the electrical signal during time and thus the control of the pressure fluctuations inside the reactor.

Fig. 2.22 Differential pressure sensor, its power supply and a connected voltmeter unit.

Fig. 2.23 The data acquisition unit.

In this way it has been possible to obtain charts showing the pressure fluctuations in the different dynamics regimes.

In particular, the interest of our study was focused on the fluctuations in entrained flow bed and slugging flow, in other words with high Reynolds numbers and important gas speeds.

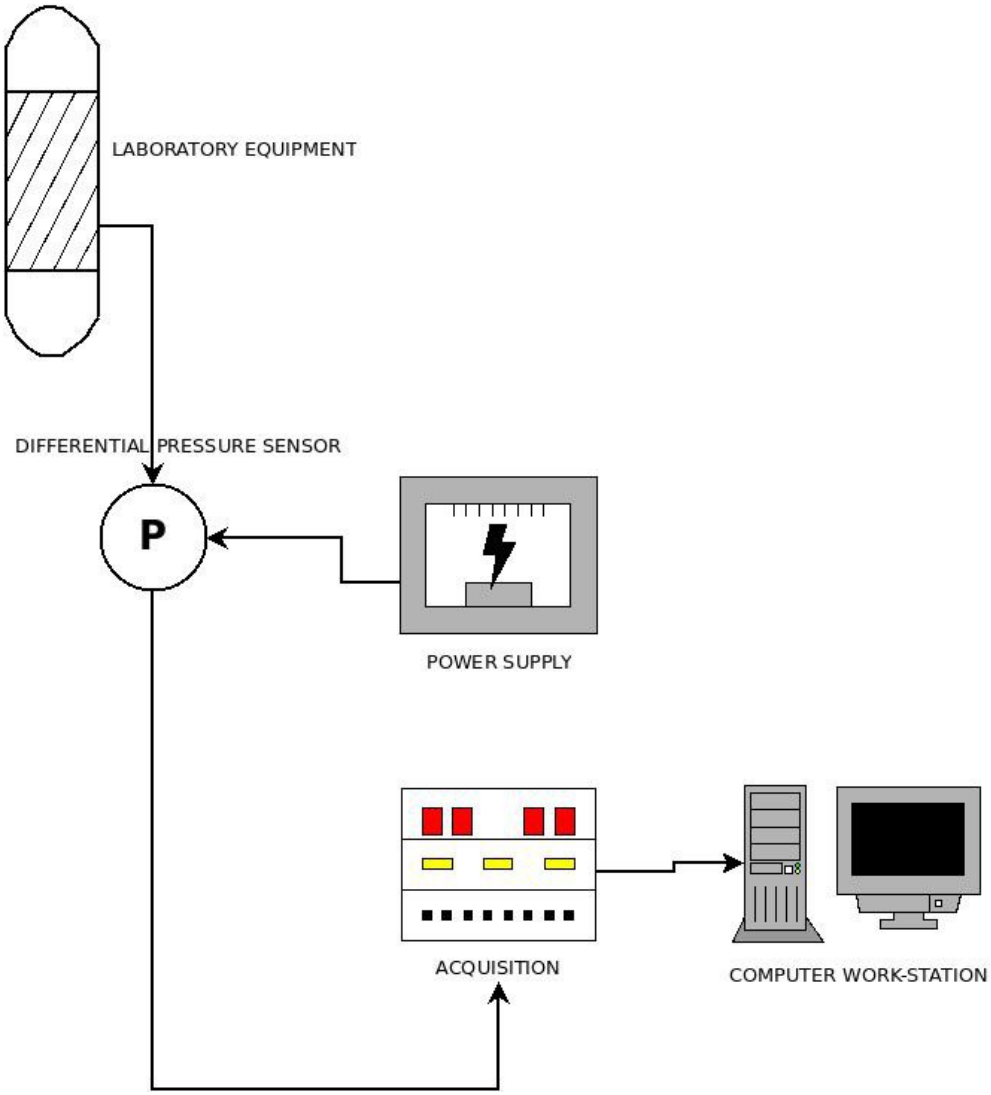

Fig. 2.24 Logical schematic of the data acquisition unit, measuring device and computer used for fluctuation detection.

In Fig. 2.24 it is shown a logical schematic of the data acquisition unit and related devices. It can be seen the differential pressure sensor with its power supply unit, the data acquisition unit which is finally connected to a computer workstation with a proper software installed.

The pressure drop measured value (the magnitude is ~1mbar) is converted to an electrical signal (the magnitude is ~100mV) and sent to the data acquisition unit.

This device has the capability to communicate in real time with the computer and plot real-

time graphics of the signal. For this project it has been chosen a 100 milliseconds time range to perform the measurement process. In this way all the small fluctuations could be detected and seen in the plot. In fact, especially in higher *Re* regimes the peaks and troughs are very narrow and close in time. For each test a set of 200 measured data has been collected in order to have a significant sample of the dynamic behavior inside the fluidized bed for a given gas speed.

2.7 Signal analysis and noise reduction

Since the measurement device is an electrical one, particular care has to be taken in considering the output electrical signal. In fact, it has been detected a small noise in the signal and this has been quantified by measuring the pressure drop within the fluidized bed not charged with any particle.
Fitting the data an equation representing the noise has been obtained. The equation obtained has a validity range limited to the operational speed which have been chosen.
In that way the equation can be used with the values of speed to obtain a value related to the noise of the instrumentation and devices. Thus, this contribution has been calculated and subtracted to the signal provided by the instrument.

The results of this calculations are plotted in Fig. 2.25 and Fig. 2.26

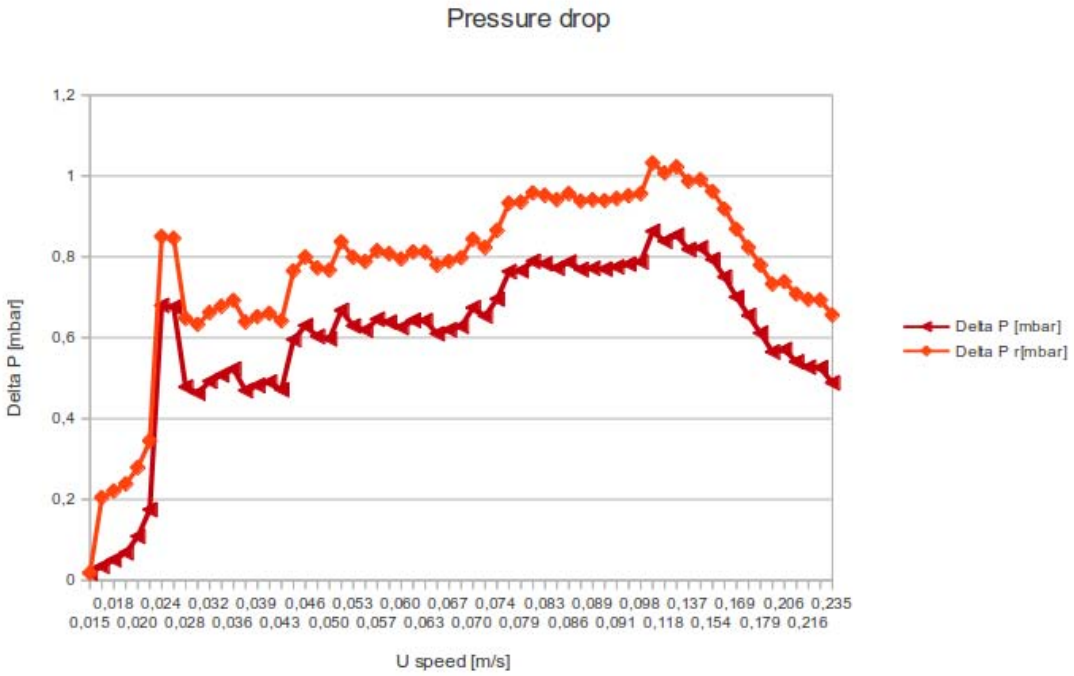

Fig. 2.25 Comparison between the pure signal (Delta P) and purified from noise one (Delta P r) (Glass spheres 12 μ).

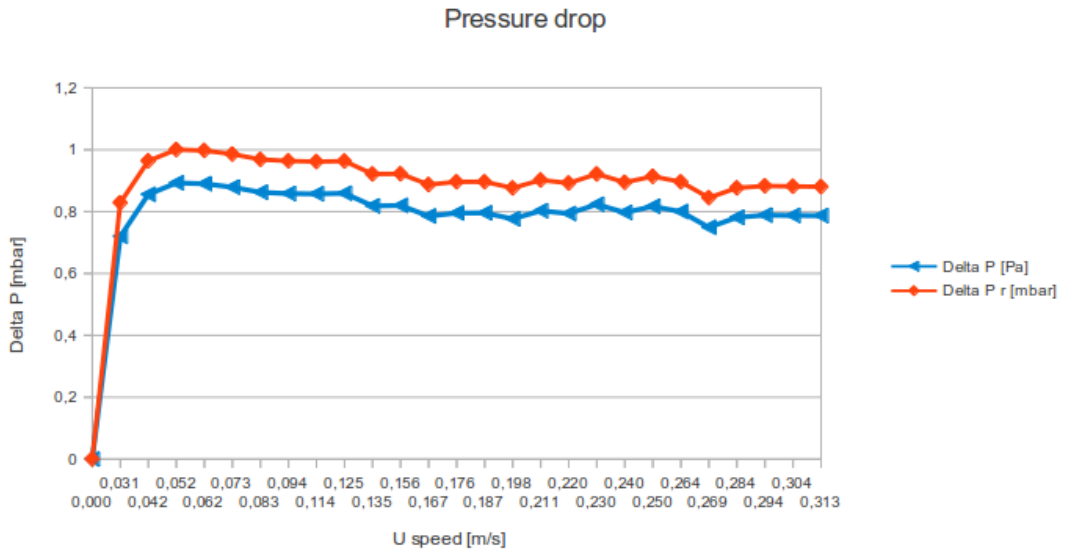

Fig. 2.26 Comparison between the pure signal (Delta P) and purified from the noise one (Delta P r) (Glass spheres 157 μm).

The previous results are analyzed in detail in section3.2.

2.8 Signal analysis with Fourier transform

To improve the results of the noise analysis previously realized, a preliminary study with Fourier transform has been performed. Since the phenomena involved in the fluidization are periodical, it is interesting to use the Fourier transform to analyze the pressure signal in detail. The Fourier Transform permits to change the data from time domain to frequency domain and thus have a sort of synthesis of the main frequency involved in the physical process, in this case, in the fluidized bed. Two preliminary Fourier analysis have been performed for the glass spheres of 157 µm diameter and 12 µm ones for minimum fluidization speed U_{mf} and for higher gas speed values.

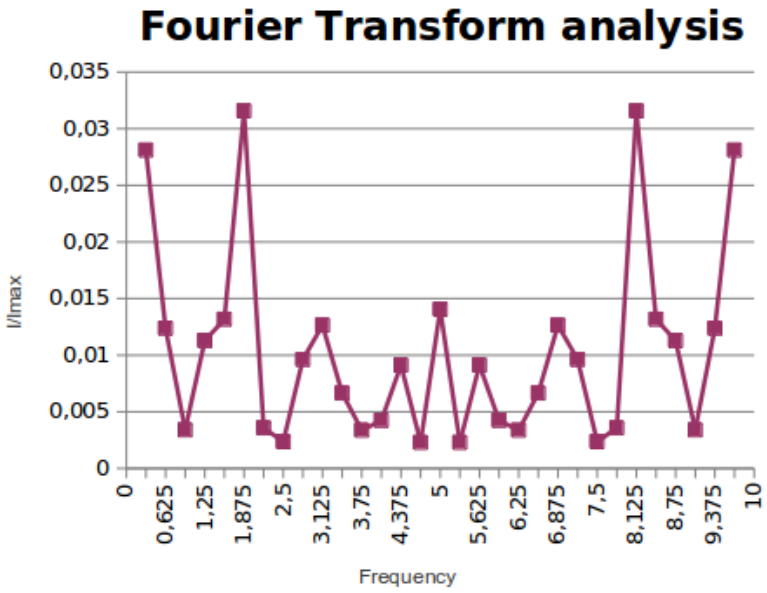

Fig. 2.27 Fourier analysis for glass spheres 12µm diameter, Gas speed=U_{mf}=0,0153 m/s.

In Fig. 2.27 it is shown the result of the Fourier transform analysis for 12 µm glass spheres in minimum fluidization conditions. At least two main frequencies (ν_1=0,3125 Hz and ν_2=1,875 Hz) can be detected in the graph and they probably represent the formation of small bubbles

in the fluidized bed. Due to its cyclical nature, the phenomenon of the bubble formation has a high number of repetition a in a period of time and thus a high frequency.

In Fig. 2.28 instead, they are reported the results for an analogue analysis for 12 μm glass spheres and a higher value for the gas speed. In this case only one main frequency can be detected (ν_f=0,3125 Hz).

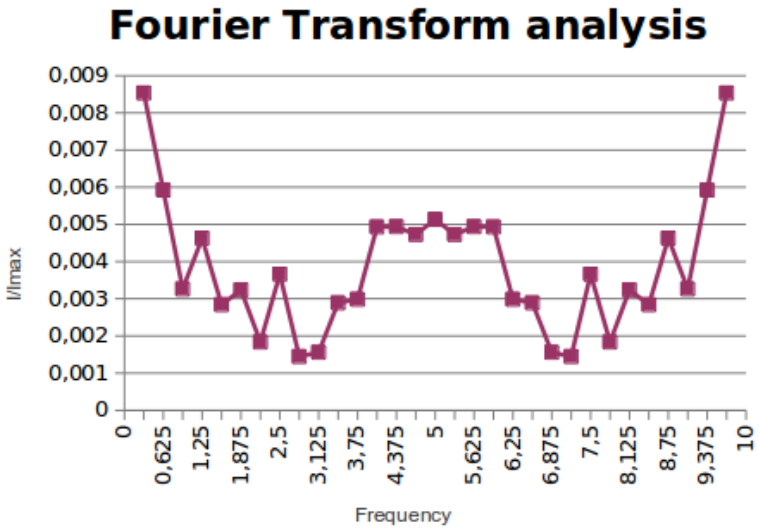

Fig. 2.28 Fourier analysis for glass spheres 12μm diameter, Gas speed=0,235m/s.

Probably when the fluidization is well developed and the gas speed is very high the formation of small bubbles becomes less evident compared to the high level of mixing and the intense movement of the bed layer.

In Fig. 2.29 it is shown the graph for 157 μm glass spheres in minimum fluidization conditions while in Fig. 2.30 it is shown the graph for the same powder with high gas speed.

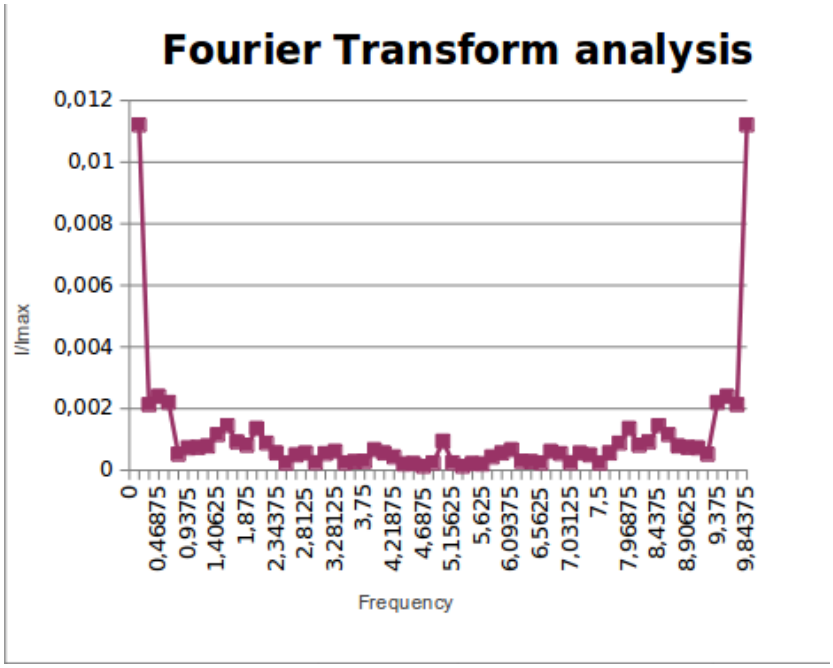

Fig. 2.29 Fourier analysis for glass spheres 157 μm diameter, Gas speed=U_{mf}=0,0225 m/s.

Comparing these two graphs, it can be noticed one main frequency in Fig. 2.29 (ν_1=0,156 Hz) while in Fig. 2.30 at least two main frequencies (ν_1=2,97 Hz and ν_2=4,38 Hz) and three secondary ones (ν_3=1,41 Hz, ν_4=2,66 Hz and ν_5=3,75 Hz) can be detected.

For the graph in Fig. 2.29, similar considerations can be done to those done for the graph in Fig. 2.27. In other words, the main frequency detected it is probably related to the formation of small gas agglomerates that coalesce in bubbles and then rise through the bed; since the gas speed is very low, this kind of phenomena is clearly evident.

Examining the peaks of the two main frequencies in Fig. 2.30, it can be said that they are probably related to the formation of two main sizes of bubbles inside the fluidized bed. The three secondary peaks can be related to smaller movements inside the fluidized bed and mixing phenomena in the dense phase.

Comparing the two couples of graphs, some differences can be noticed. First of all working with 12 μm glass spheres, the peaks in the graph are fewer and less evident. This can be due

to the cohesive nature of the powder which limits the movements inside the solid phase; in fact these material is classified C by Geldart . Since the 157 μm glass spheres belong to B Geldart's group, they are not cohesive and thus, the movement inside the solid phase are easier.

The lower frequencies shown in the graph which have not been classified as important are probably related to the noise of the instrumentation. A future development could implement a filter to eliminate this kind of frequencies and thus have a signal purified by the noise.

Due to lack of time in the working period, this step has not been performed but it could be an interesting future development.

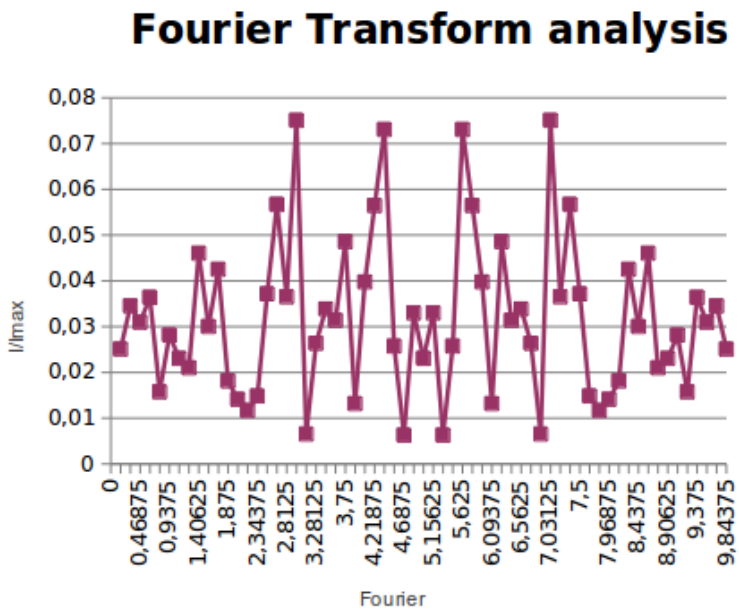

Fig. 2.30 Fourier analysis for glass spheres 157 μm diameter, Gas speed=0,3135m/s.

3 CHAPTER THREE
HYDRODYNAMIC STUDY FOR DIFFERENT KIND OF POWDERS: THE RESULTS

3.1 Fluid dynamics tests in fluidized bed regime

3.1.1 Variation of the pressure drop versus increasing gas speed

As a first step, using the first prototype, it has been possible to set up a set of measurements of the pressure drop in the fluidized bed varying the amount of air which was sent inside the fluidized bed itself. Then, a second set of measurements has been taken with the second prototype. From the data collected it has been possible to draw two curves: the first one (marked in red, triangles) is related to the data collected increasing the speed from 0 m/s to 6,285 m/s and the second one is related to the data collected during the reverse path (marked in blue, diamonds).

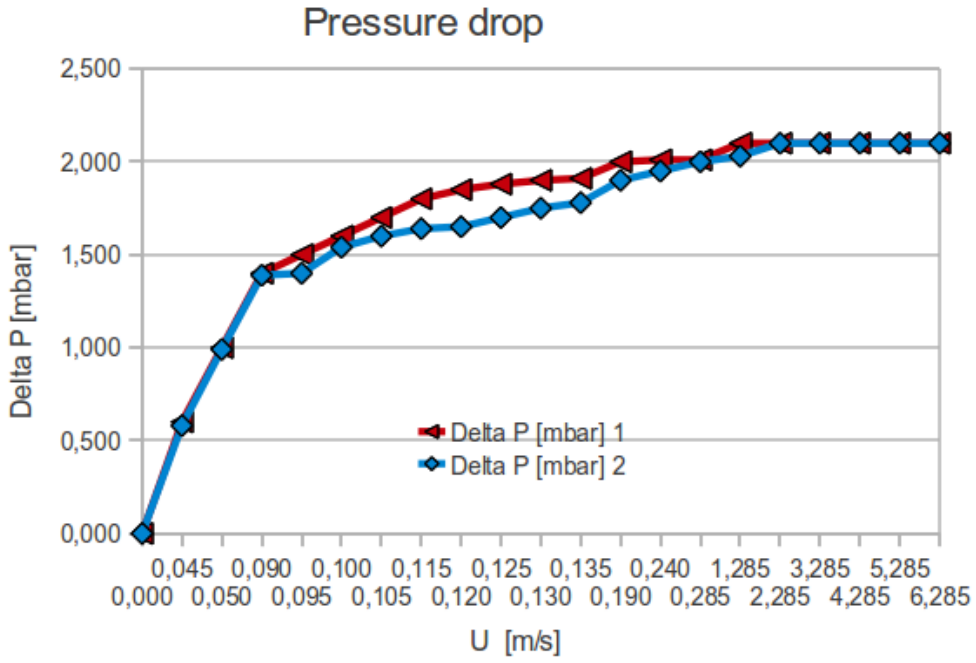

Fig. 3.1 Pressure drop in the fluidized bed with 340 μm glass powder

As shown in Fig. 3.1 there is a slight difference between the two curves; in particular the lower values in the second curve can be due to some material losses during the

experiment. Measuring the weight of the samples before and after each experiment it has been calculated that the massive amount of powder which was found in the collecting tank or small traces that remained inside the porous filter was lower than 0,65% of the previously charged amount. In this way, it can be said that massive losses are negligible and can not explain the difference between the two curves.

In fact, a more interesting reason to explain the situation in the previous graph can be found in hysteresis phenomena. For lower ranges of U, we are in the fixed bed regime and the powder is packed. In order to overcome the cohesive forces which keep the particles tight, it will be necessary an higher amount of energy than the one experienced in the reverse path. In other words, if we start from a bed which is already well fluidized the amount of energy (and thus the measured pressure drop) will be lower than the one needed starting from a packed bed.

Moreover, on the basis of the collected data it has been possible to perform a comparison between the calculated value of U_{mf} and the measured one.

It can be noticed that the curve has two main parts: the first one has a pronounced slope and it corresponds to speed values lower than the U_{mf}; the second one shows speed values to which the particles are involved in gas transport.

The measured value for U_{mf} can be obtained approximating the first part of the curve as a straight line and finding the intersection with the same approximation for the second part of the curve (see Fig. 3.2).

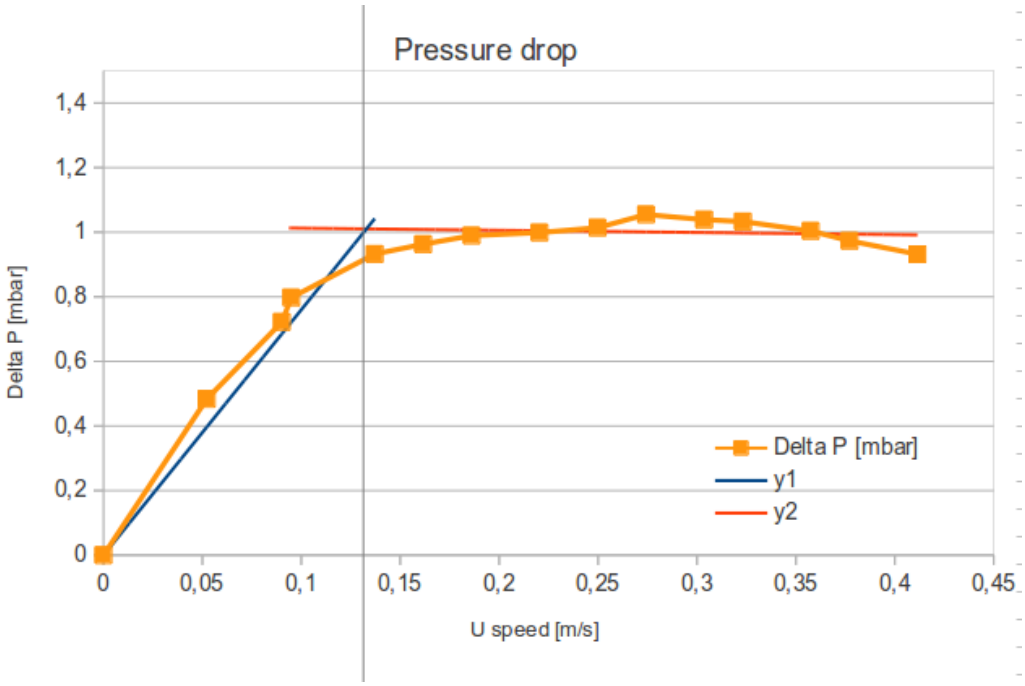

Fig. 3.2 Fitting experimental data to find the measured value for Umf (340 μm).

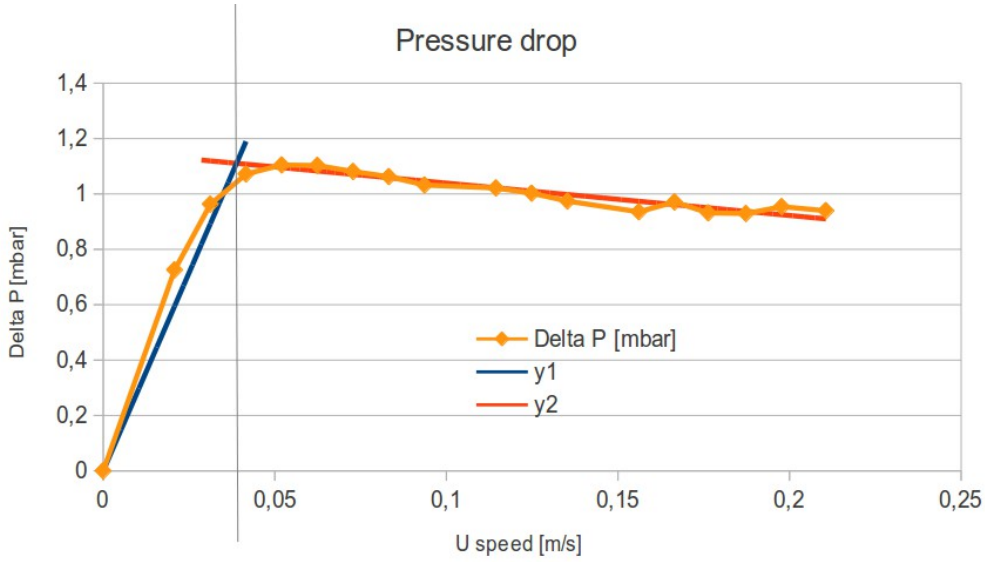

Fig. 3.3 Fitting experimental data to find the measured value for Umf (157 μm).

Comparing the experimental value for U_{mf} and the one evaluated through the formulas (6) and

then (7), it can be calculated the relative error e_r, average value $\bar{e}_r$ and variance σ_e^2 as follows:

$$e_r(\%) = \left| \frac{U_{mf}^{\exp} - U_{mf}^{WY}}{U_{mf}^{\exp}} \right| \cdot 100 \qquad (15)$$

$$\bar{e}_r = \frac{\sum_{i=1}^{n} e_{r,i}}{n} \qquad (16)$$

$$\sigma_e^2 = \frac{\sum_{i=1}^{n} (e_i - \bar{e}_r)^2}{n} \qquad (17)$$

Tab. 3.1: The results of calculated and experimental values for U_{mf} and related error e_r, average value $\bar{e}_r$ and variance σ_e^2.

	Diameter [μm]	***Density [kg/m³]***	***U_{mf}^{WY} [m/s]***	***U_{mf}^{exp} [m/s]***	***e_r (%)***	***$\bar{e}_r$***	***σ_e^2***
Glass spheres 3	340	2640	0,0950	0,1437	33,9	34,25	0,1225
Glass spheres 3	340	2640	0,0950	0,1452	34,6		
Glass spheres 2	157	2640	0,0208	0,0388	46,4	47,75	1,8225
Glass spheres 2	157	2640	0,0208	0,0409	49,1		

During the experiments it could be observed that there was a significant difference between the two values of U_{mf}. In fact from the results of the test e_r showed values ranging from 33,9%÷34,6% for 340 μm glass spheres, up to 46,4÷49,1% for the 157 μm ones (see Tab. 3.1).

As stated by Fei Wang and Liang-Shih Fan [13], this difference can be explained by the additional pressure drop due to the wall effect in the microfluidic channel.

The wall effect can be very relevant, in fact, Wang & Fan using Wen & Yu relation (7) experienced huge offset so that: $U_{mf}^{\exp} = 3 \div 5 \, (U_{mf}^{WY})$.

3.1.2 Fluctuations of the pressure drop during time

The previous graphs (Fig. 3.1 and Fig. 3.2) has been the starting point to a second phase for the analysis. In fact, some specific values of U have been chosen to investigate different flow regimes in the fluidized bed. Therefore, the fluctuations in the pressure drop along time were measured for each of these values of gas speed. As shown in Fig. 3.5 for the fixed bed, the fluctuations are very small and we can assume the pressure drop is constant, while in Fig. 3.8 and Fig. 3.10 , for higher values of gas speed, they begin to be easily detectable. In Fig. 3.11 it is shown a photograph of the prototype in fluidized bed regime.

In particular, in Fig. 3.12 and Fig. 3.13, the *slugging flow regime* can be identified as each variation in the pressure drop indicates a bubble passing through the particles layer (Fig. 3.4). In fact, on the top of each bubble it can be measured a value P_1 for the low pressure zone of the sphere while in the lower part of each bubble a value $P_2 > P_1$ for the high pressure zone can be measured. The difference $\Delta P_{bubble} = P_2 - P_1$ is, indeed, the driving force that permits to the bubble to raise through the fluidized bed.

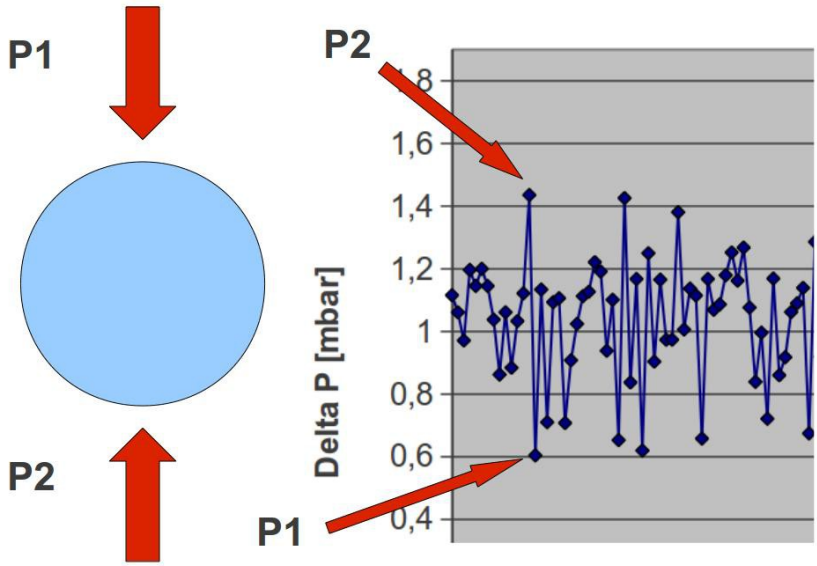

Fig. 3.4 The zones corresponding to high and low pressure values can be detected respectively from the fluctuation peaks (P2) and troughs (P1) .

In this way, we can assume that, examining two values of the pressure drop which are one next to the other, they represent the passage of one bubble in the bed, as they are the lower and the higher values of the driving force for that single bubble.

Hence, the larger the fluctuations, the higher will be the Reynolds number and the flow regime in the bed will tend to entrained bed one. Moreover, it can be said that the dimension of the bubbles is related to the magnitude of the fluctuations. Observing the graphs of pressure drop it can be noticed also a limited range of smaller fluctuations; these represent the solid phase which is put in movement by the gas flowing in. The fluctuations related to the passage of a bubble exceed this band limiting the signal representing the particle phase.

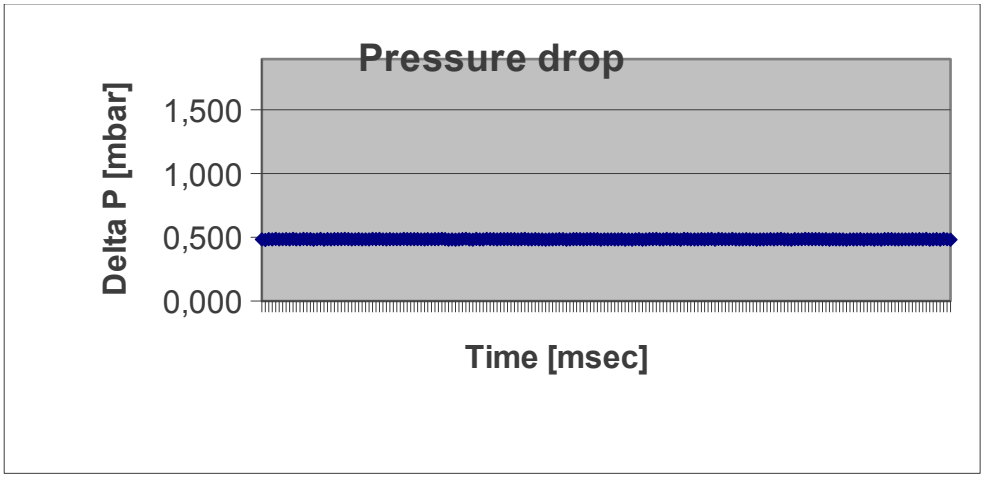

Fig. 3.5 Fluctuations in fixed bed: the value of pressure drops is almost constant (340 μm, U=0,052 m/s, H=1,4cm)

In Fig. 3.7 we can see a particular of the fluctuations in the fixed bed regime; if they are compared to the ones in entrained bed (Fig. 3.12) they can be neglected but, examining the graph in detail it can be seen that there are some variations.

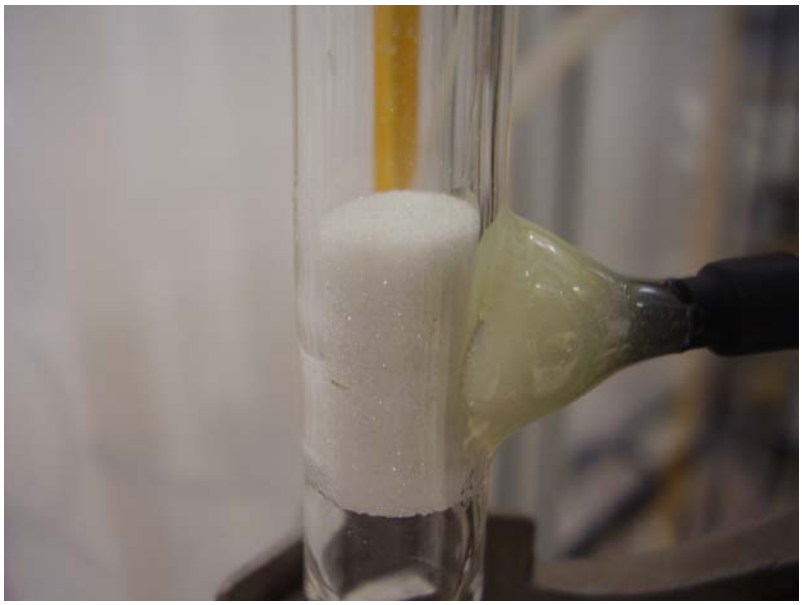

Fig. 3.6 Photograph of the second prototype in fixed bed regime.

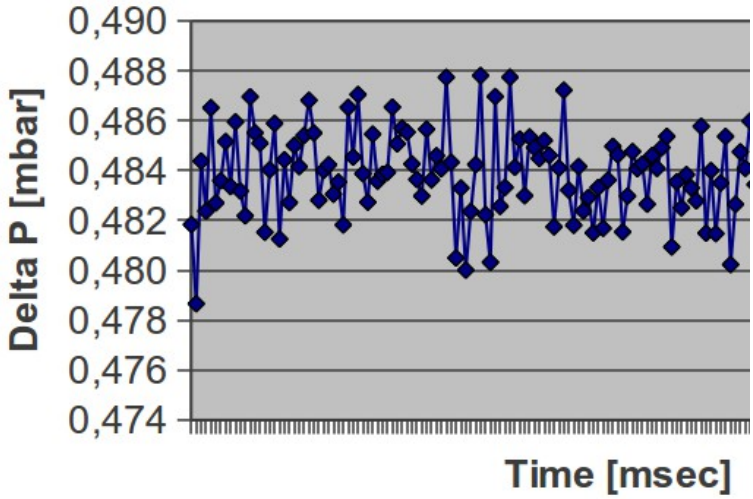

Fig. 3.7 Particular of the fluctuations in fixed bed:the values are between 0,478 and 0,489 mbar (340 μm, U=0,052 m/s, H=1,4cm).

In Fig. 3.5 and Fig. 3.6 it is showed the fixed bed regime: the powder stands still, letting the gas flow through the spaces between the particles. The bed has a height called minimum height H_0.

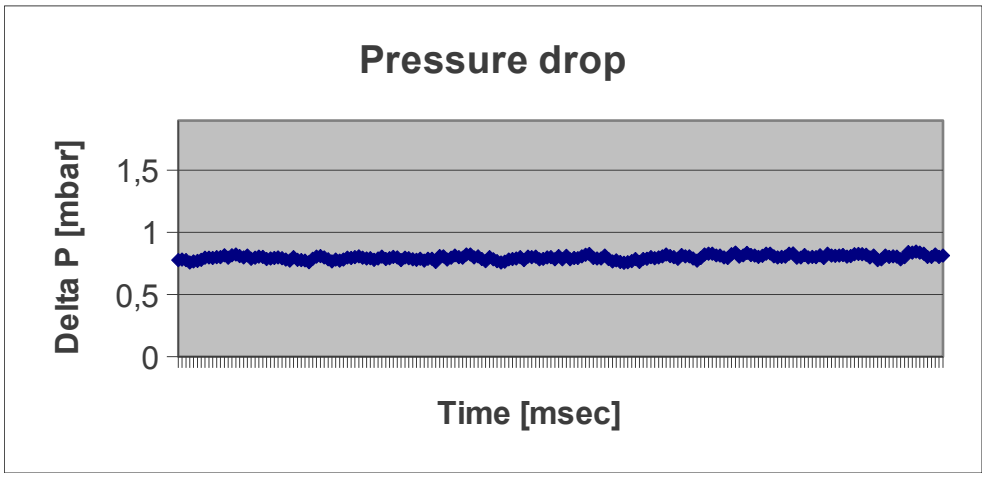

Fig. 3.8 Fluctuations in fluidized bed: the value of pressure drops begins to show slight variations (340 μm, U=0,095 m/s, H=1,4cm)

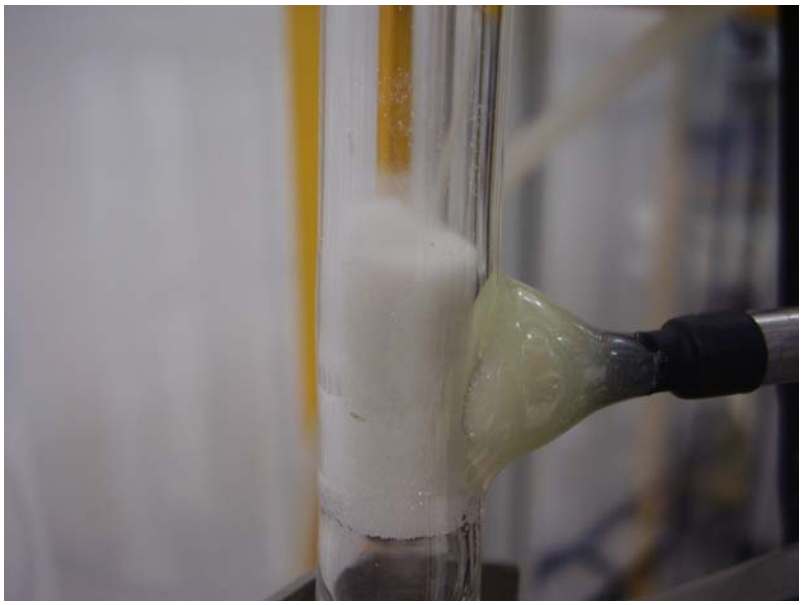

Fig. 3.9 Photograph of the second prototype in weakly fluidized bed regime.

In Fig. 3.9 it can be seen that the bed has increased its height; when the air is sent in with a flow rate corresponding to U_{mf}, the bed reaches the minimum fluidization height, H_{mf}.

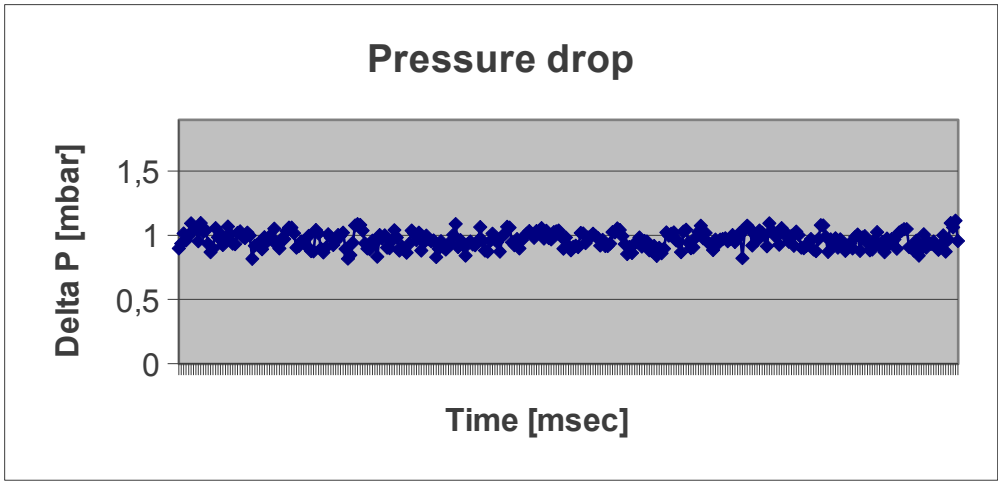

Fig. 3.10 Fluctuations in fluidized bed: the value of pressure drops begins to show higher variations (340 μm, U=0,109 m/s, H=1,4cm)

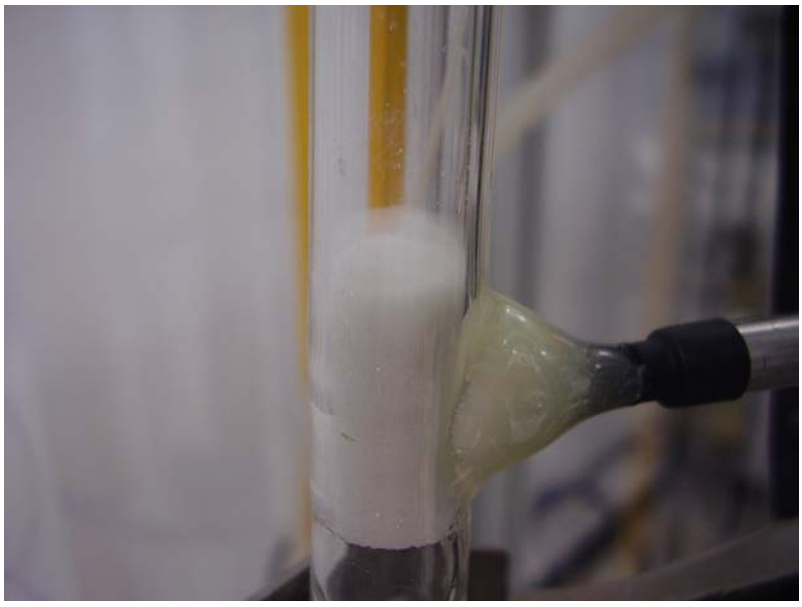

Fig. 3.11 Photograph of the second prototype in fluidized bed regime.

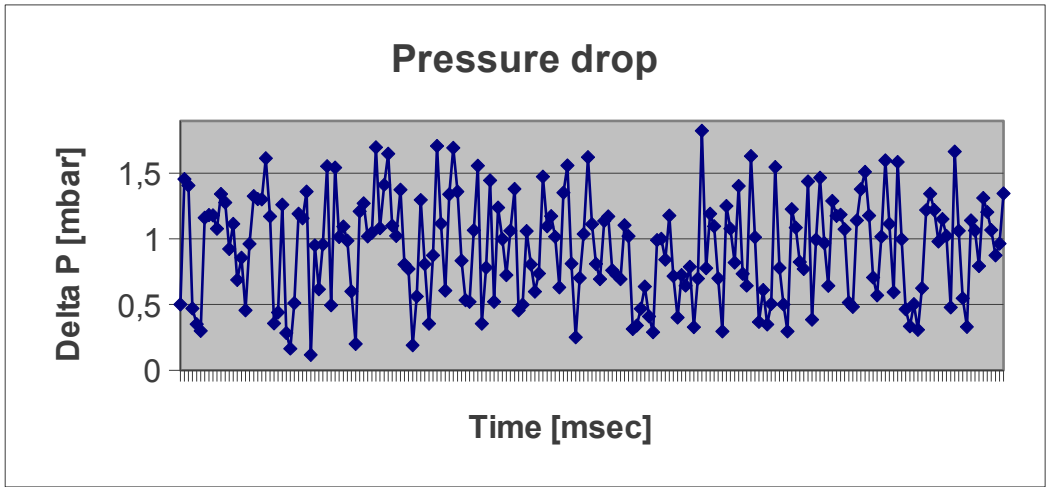

Fig. 3.12 Fluctuations in entrained bed: the value of pressure drops shows important variations (340 μm, U=1,285 m/s, H=1,4cm)

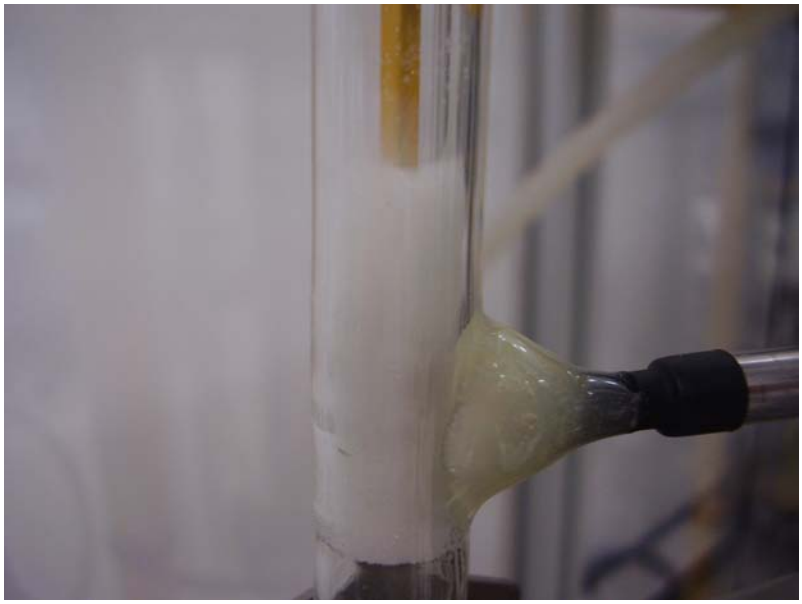

Fig. 3.13 Photograph of the second prototype in entrained bed regime.

Comparing Fig. 3.6, Fig. 3.9, Fig. 3.11 and Fig. 3.13, it is clearly identifiable the bed expansion for gas speed increasing and the differences between the four flow regimes.

3.2 Graphical analysis of the pressure drop signal

In Fig. 3.14 it is showed the analysis for the pressure drop curve; it has been divided in different significant zones and then these zones have been qualitatively analyzed.

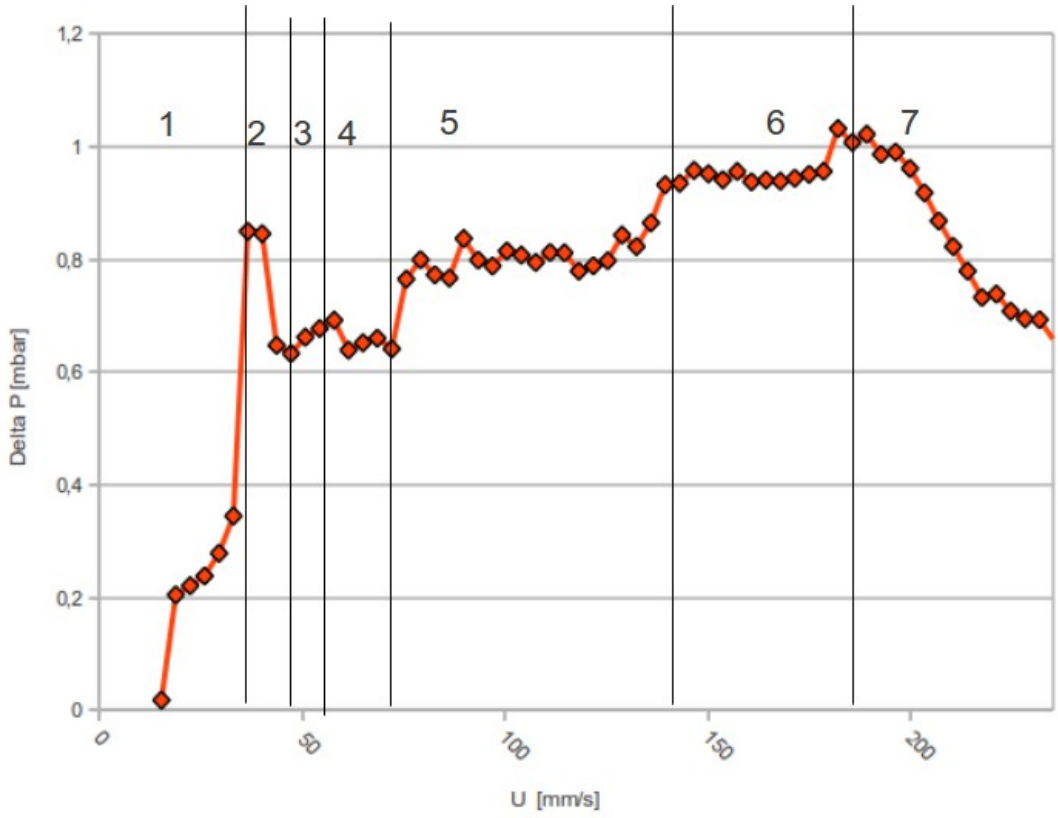

Fig. 3.14 Analysis of the different phenomena in the pressure drop curve for different gas speed. (Glass spheres 12 μm)

In zone number **1** it is represented the fixed bed regime: here only small clusters begin to be fluidized. In the second zone, after the peak it can be detected that those agglomerates have been disaggregated. In zone **3** larger clusters begin to move for the action of the gas flowing through the bed. In zone **4** a fall can be noticed after the braking of medium size clusters. In the same way in zones **5** and **6**, bigger clusters are fluidized and then disaggregated. Finally, In the **7**th zone an important fall in the signal is detected. This can be caused by the mass losses due to entrainment of the last particles.

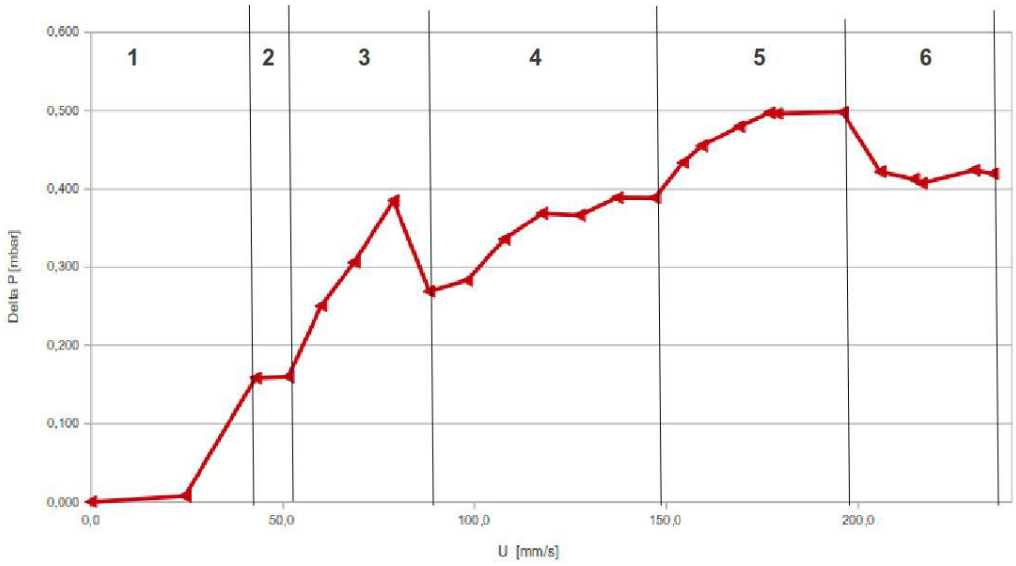

Fig. 3.15 Analysis of the different phenomena in the pressure drop curve for different gas speed. (TiO_2 , 360 nm).

Similarly in Fig. 3.15 it is showed a graph for the pressure drop curve for the TiO_2; in the same way, it has been divided in different zones and then a qualitative analysis has been performed. In zone number **1** it is represented the fixed bed regime: here only small clusters begin to be fluidized. In the second zone, a small plateau can be detected and so the pressure drop is constant. This can be due to a lack of energy from the gas sent in, in other words, the gas speed was sufficient to put in fluidization only small agglomerates, but it is not high enough to entrain bigger ones.

In zone **3** larger clusters begin to move for the action of the gas flowing through the bed; after the peak the deagglomeration of those agglomerates can be detected. In zone **4** after the fall, it can be noticed the fluidization of medium size clusters. In the same way, in the **5th** zone, bigger clusters are fluidized and finally disaggregated in the **6th** zone, where an important fall in the pressure drop value is detected. Again, this can be caused by the mass losses due to entrainment of the last particles. Some differences can be noticed between this curve (see Fig. 3.15) and the one related to the glass spheres of 12 μm diameter (see Fig. 3.14). The different hydrodynamic behaviour of the TiO_2 is related to its strong cohesive forces.

3.3 Fluid dynamics tests in slugging regime

While increasing the gas speed during the tests, different flow regimes were detected. In particular due to the cohesive nature of some powders (especially Talc and TiO_2) the bed showed a particular behaviour called *slugging*. In this flow regime the drag forces are sufficient to transport the powder upward, but at the same time they are lower than the cohesive forces. In this way the solid phase is divided in clusters which are transported as units composed of a multitude of particles. At this point the nominal average value for the diameter can no longer be considered as a valid measure for the powder in use. Indeed, an apparent value for the diameter must considered in order to take into account the cohesive force contribution. This phenomenon can be expressed as well with the ratio between the measured value of U_{mf} and the value calculated through Wen & Yu relation (7):

$$speed\ ratio(\%) = \frac{U_{mf}^{\exp}}{U_{mf}^{WY}} \cdot 100 \qquad (18).$$

This ratio has been calculated for several powders and, just to give an idea, during the tests it has been equal to 131 for the glass spheres and to $4{,}20 \cdot 10^6$ for the TiO_2.
When the slugging regime occurs the measuring process of the pressure drop can be difficult. In fact, sharp fluctuations can be observed in the values of the pressure drop and in that way it can be very difficult to determine which is the actual value for ΔP for a given U.

3.4 Scale-down considerations

Some preliminary calculations have been performed to chose the best value for the diameter of the following prototype. In order to better understand the flow regime in the future reactor to be built, the Reynolds number has been calculated for different gas speeds; this has been done decreasing the reactor diameter to see how this parameter could have influenced the dynamics of the fluidized bed.
As a reference, the values shown in Tab. 3.2 have been considered for the air and the particles.

Tab. 3.2 Reference values for the dynamics calculations.

Air	***Glass spheres***		
μ_g ***[Pa · s]***	ρ_g ***[kg/m^3]***	D_p ***[m]***	ρ_p ***[kg/m^3]***
$1{,}85 \cdot 10^{-5}$	1,21	$3{,}4\ 10^{-4}$	2640

Here, only the results for the 340 μm glass spheres are shown, but similar results have been obtained for the other powders. Again, after calculating Archimedes number via equation (8), Reynolds number has been evaluated through Wen & Yu relation (7) and finally the value of U_{mf} was obtained.

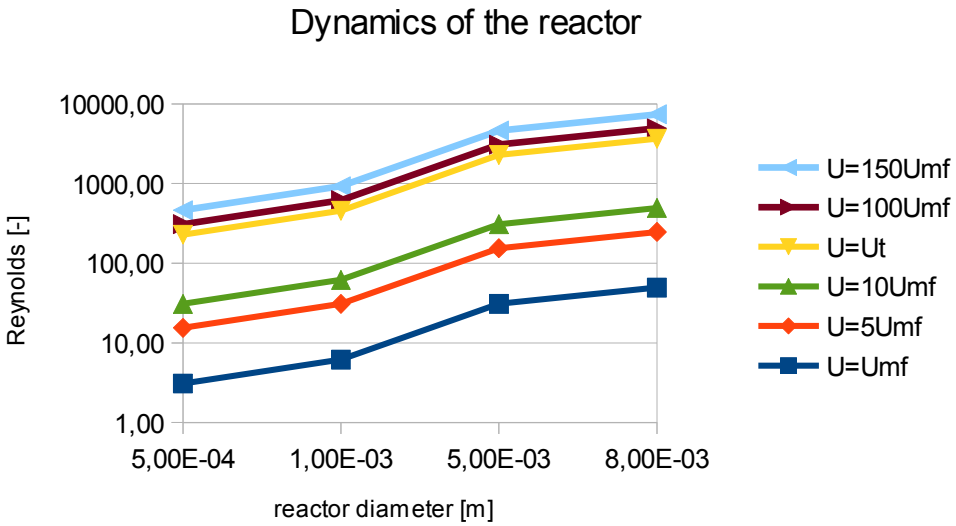

Fig. 3.16 Reynolds number vs reactor diameter for different values of the gas speed (log scale, reference powder: glass spheres 340μ).

As can be seen in Fig. 3.16 different values of gas speed have been taken into account: the minimum fluidization speed U_{mf} (and several multiples of it) and the limit speed U_t. The chart shows that it is necessary to choose an enormous value to exceed the limit speed value:

$$U = 100 \cdot U_{mf} \rightarrow U > U_t \quad .$$

In practical operating conditions, it is recommended not to exceed this value U_t to prevent the particles to be entrained out of the experimental device.

4 CHAPTER FOUR
FUTURE IMPROVEMENTS

The first aspect that could be studied in the future is certainly the study of the hydrodynamics inside the third prototype. The tests have not been performed only due to lack of time during the experimental work. The third prototype could have been realized only in the last days of the experimental work.

Moreover, a heat transfer study and numerical simulation could be performed as future improvements to investigate other aspects of the micro fluidization devices.

Among the different options for future improvements that have been examined, one seems particularly interesting. Working with a wide particle size distribution powder mixture, different flow regimes could be obtained in the same reactor.

Now, if we have a distribution in particle diameters similar to the one in Fig. 4.1, in other words, if we have different diameters coexisting in the sample of powder we are working with, we will observe several behaviors in the flow dynamics.

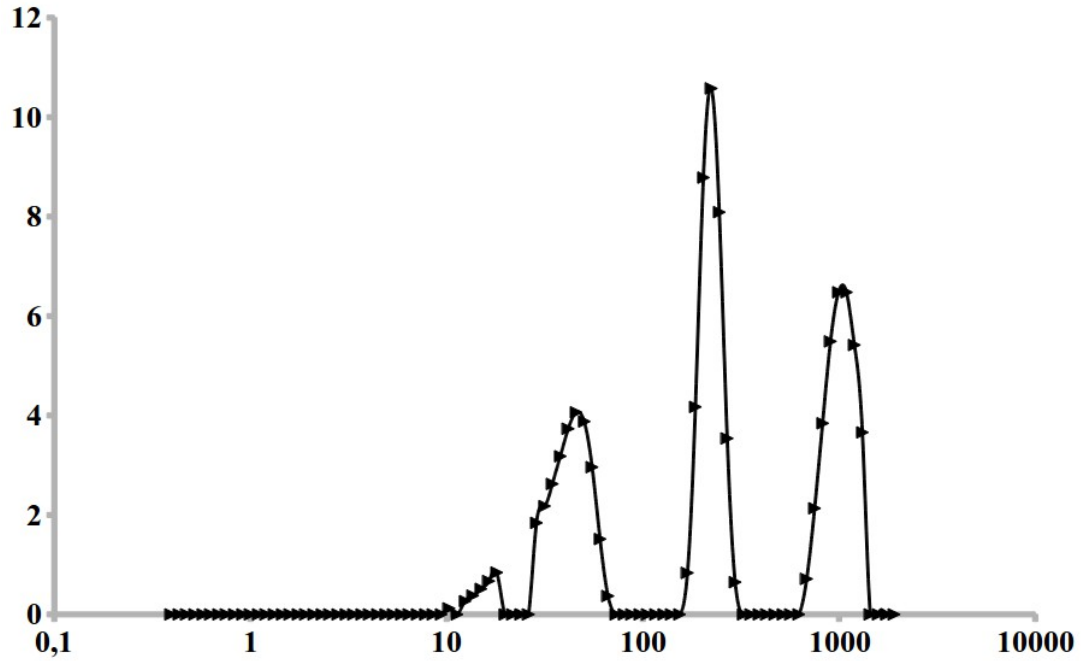

*Fig. 4.1*An example of a sample of powder in which several diameters are present with different percentage (all measures expressed in [μm].)

In fact, for a given flow rate of air, powders having different diameters will behave differently. In particular, it can be assumed that the particles with lower diameter will reach easily entrained bed flow regimes, while the other particles with bigger diameters will be in a weak fluidization regime.

For example, if we work with a mixture of powders having three main diameters, say $d_1<d_2<d_3$, we can assume that it would be possible to obtain three layers of fluidization each one corresponding to a different flow regime (see Fig. 4.2).

In this way we can obtain three different layers of powders segregated according to their diameter. In an industrial application, for example, each layer could correspond to a different phase of a chemical process or to a different step of a reaction.

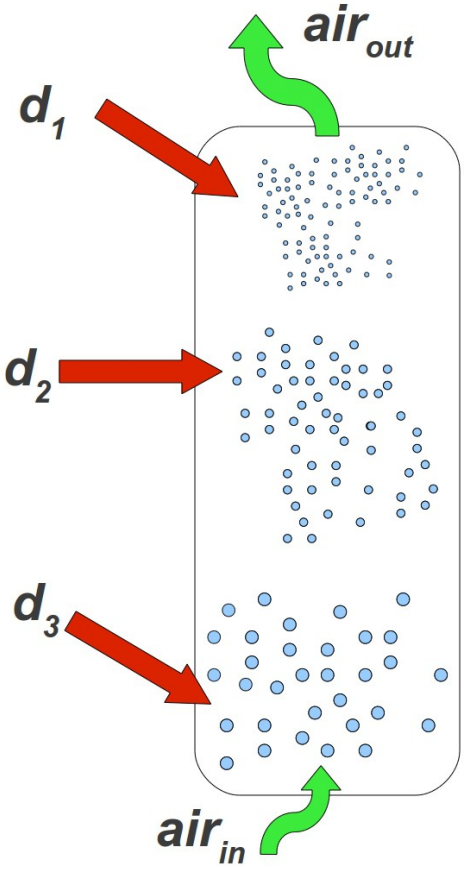

Fig. 4.2 Working with powders having three different diameters: three segregated layers of fluidization can be obtained.

Hereafter we will describe other future purposes for the micro-reactor object of our study.
The MicroGasic reactor has been conceived as a microfluidic system for gas-solid reactions and it will be used for the suspension or dispersion of nanometric powders (with a diameter lower than 200 nm) achieving very high values for the gas speed inside the micro tubes.
Moreover, the dispersion of particles and the contact between these will be carried out in tubes with dimensions lower than 10 μm. For that reason, the reactor will have a very complex configuration and an innovative design.

However, the most important and complex problems are related to the deagglomeration and separation of nanometric powders and to the appropriate design of the MicroGasic system.

The very low size of the tubes makes it possible to obtain high gas speed and a turbulent flow which allows a better shearing of the agglomerates and the dispersion of the nanometric particles. Furthermore, the design of the microgasic process allows good dispersion, good gas-solid mixing and, finally, better separation of gases and the solid at the end of the reaction.

5 CHAPTER FIVE
CONCLUSIONS

The experimental work has been done mainly with powders which present a dynamic behaviour which is not difficult to manage compared to some powders of the group C of Geldart classification criterion. This choice has been necessary for a first phase of the project: the implementation of the micro-fluidized bed.
Some interesting results were obtained with regards to the curves of fluidization and to the values of minimum fluidization speed U_{mf}.
It has been possible to achieve high values of fluidization quality up to:

$$fluidization\ quality = \frac{\Delta P}{W / A} = 97\%$$

Moreover, it has been possible to realize a diagnostic system through the measurement of fluctuations in the pressure drop.
About 10'000 pressure measures have been taken for each test for a given value of gas speed, so that a wide range of fluctuations could have been explored.

The method has proven to be suitable especially for micrometric and sub-micrometric powders and it is useful to realize the identification of the flow regime through the fluctuations of the pressure drop signal. This permits to better understand the hydrodynamics inside the column and makes it possible to avoid inconvenience of the fluidization such as channeling, slugging and the solidification of the powder in the bed. In fact, this phenomena can be detected from the analysis of the peaks and of the shape of the fluidization curves.

This kind of diagnostic can be interesting especially in lower scales, where the phenomena running inside the vessel can not be easily detected with traditional techniques.
After these results have been obtained, two powders of the C Geldart's group have been studied: 12 μm glass spheres and TiO_2. Due to the purpose of the project to lower the scale of

the laboratory equipment and the diameter of the particles studied it has been necessary to work with powders which are not used in general for fluidized beds.
Even if the experiments were performed with powders which are not suitable for the fluidization, some good results have been obtained in terms of fluidization quality and further analysis of the fluidization curve.

The results obtained with the second prototype (with 8,5mm internal diameter) have been very encouraging and were taken as a basis for the design procedure of the third prototype (with a channel of 1mm internal diameter).
Although this process has real challenges, i.e. the complexity of the flow dynamics and the very cohesive powders, it shows many advantages such as the capability of making the gas and the active product react together without a support material, the absence of friction (thus avoiding fragmentation, abrasion and chipping) between the particles and the increase of the heat transfer surface and of the thermal stability of the whole reactor.

5.1 Notes *to Tab. 1.1*

D_r	diameter of the reactor [mm]
D_p	diameter of the particles [mm], [cm], [μm]
ε	voidage of the packed-fluidized bed [-]
H_{fc}/D_r	aspect ratio [-]
H_{fc}	confined bed height [cm]
T_b	temperature of the bed [°C]
U_t	terminal velocity [mm/s]
U_{mb}	minimum bubbling velocity [mm/s]
U_{mf}	minimum fluidization velocity [mm/s]

BIBLIOGRAPHY

1: D.Geldart, Types of gas fluidization, 1973

2: User A1, Diagram of a fluidised bed, 2008

3: arab-eng, www.arab-eng.org, 2013

4: Richard G. Holdich, Fundamentals of Particle Technology, 2002

5: K. S. Lim, J. X. Zhu, J. R. Grace, Hydrodynamics of gas-solid fluidization, 1995

6: Clift R., An Occamist review of fluidized bed modelling, 1993

7: R. Clift, S.Rafailidis, Interparticle stress, fluid pressure and bubble motion in gas-fluidized beds, 1993

8: B. Potic, S.R.A. Kersten, M. Ye, M.A. van der Hoef, J.A.M. Kuipers, W.P.M. van Swaaij, Fluidization with hot compressed water in micro-reactors, 2005

9: Xinhua Liu, Guangwen Xu, Shiqiu Gao, Micro fluidized beds: Wall effect and operability, 2007

10: Ma Jiliang, Chen Xiaoping, Liu Daoyin, Minimum fluidization velocity of particles with wide size distribution athigh temperatures, 2012

11: Rossella Girimonte, Vincenzino Vivacqua, Design criteria for homogeneous fluidization of Geldart's class b solidsupward through a packed bed, 2013

12: Wen, C.Y. and Yu, Y.-H., A generalized method for predicting theminimum fluidization velocity, 1966

13: Fei Wang, Liang-Shih Fan, gas-solid fluidization in a microfluidic channel, 2011

Acknowledgements

I would like to thank prof. Nouria Fatah, my French supervisor during the whole experimental work; it has been always a pleasure to work together and coping with inconveniences of the set-up was a challenge which we faced with determination and effort, but thanks to a friendly work environment, it seemed to me less hard.

I would like to thank prof. Andrea Santomaso, my Italian supervisor, for his helpful advices; in spite of some difficulties in communication due to the distance, I had kind and useful support.

I would like to thank, Laurent D'Apolito, *maître verrier,* for his helpful work in blowing all the glass prototypes we needed and for his pleasant irony.

I would like to thank also Gérard Cambien et Johan Jezequel, for their kind help in the laboratory and all the young researchers with whom I spent wonderful days in the laboratory and at lunch time: David Roger Melendez Guevara, Jorge Alonso Delgado Delgado, Guido Chiappori, Diego Peña, Luca Iozzelli, Fabien Grasset, Unai De la Torre and Javier Ibáñez.